Download PDF: 01.04.2026

ETH-Bibliothek Zürich, E-Periodica, https://www.e-periodica.ch

Assessment of the Remaining Fatigue Life of Defective Welded Joints

Evaluation de la durée de vie restante de joints soudés défectueux

Abschätzung der Restlebensdauer schadhafter Schweissverbindungen

O.D. DIJKSTRA
Civil Engineer
TNO-IBBC
Delft, The Netherlands

Onno Dijkstra, born 1945, received his civil engineering degree at the Delft University of Technology. He has been involved in fatigue and fracture mechanics since 1974. Onno Dijkstra is now in the Steel Department of TNO-IBBC and is responsible for fatigue and fracture mechanics research.

H.H. SNIJDER
Civil Engineer
Netherlands Railways
Utrecht, The Netherlands

Bert Snijder, born 1959, obtained his civil engineering degree at the Delft University of Technology. For five years, he was involved in steel structures research at TNO-IBBC. Topics of interest include stability and fatigue. Bert Snijder is now in a design office and is responsible for the design of steel buildings and bridges.

H.J.M. VAN RONGEN
Senior Scientist
TNO Metals Research Inst.
Apeldoorn, The Netherlands

Bob van Rongen, born 1933, received his physics degree at the University of Leiden. He has been involved in fracture mechanics since 1972. Bob van Rongen is now in the welding and materials department and is responsible for the use and dissemination of fracture analysis methods.

SUMMARY
This paper deals with the determination of the remaining fatigue life of defective welded steel structures. Highlighted are defect schematization and recategorization, crack-growth laws and their constants, stress-intensity-factor solutions for welded joints and a fatigue crack-growth calculation procedure. The information given can be used for two dimensional and three dimensional welded geometries.

RÉSUMÉ
Cet article traite de la détermination de la durée de vie restante de structures soudées en acier contenant des défauts. L'accent est mis plus particulièrement sur la schématisation et la classification des défauts, sur les lois de propagation des fissures et leurs constantes, sur les valeurs du facteur d'intensité de contraintes pour des joints soudés, et sur la procédure de calcul de la propagation des fissures de fatigue. L'information présentée ici peut être utilisée pour des géométries d'éléments soudés bidimensionnels et tridimensionnels.

ZUSAMMENFASSUNG
Dieser Bericht befasst sich mit der Bestimmung der Restlebensdauer geschweisster Stahltragwerke, die Schäden aufweisen. Beleuchtet werden die systematische Darstellung und Klassierung von Schäden, Rissfortschrittsgesetze und deren Konstanten, Spannungsintensitätsfaktoren für Schweissverbindungen sowie ein Verfahren zur Berechnung des Ermüdungsrisswachstums. Alle Angaben sind sowohl für geschweisste Verbindungen zweidimensionaler als auch für solche dreidimensionaler Geometrie gültig.

1. INTRODUCTION

Steel structures may contain defects in the (welded) connections. These defects can be discovered directly after fabrication by non destructive testing or during service by inspection. Repair of these defects is often costly and time consuming. The costs may be extremely high when an existing structure has to be taken out of service or when the use of a new structure is delayed. Furthermore, a repair of a structure has to be carried out in an unfavourable situation with regard to the accessibility and restraint. Therefore, these repairs are often not beneficial to the integrity of the structure.
The above mentioned reasons make that a "fitness for purpose" assessment of a defective joint may be useful and may lead to the conclusion that the safety of the structure is not reduced by the presence of the defect discovered. In a statically loaded structure an assessment of the risk of instable (brittle) fracture initiated from the defect discovered is sufficient. However, for a fatigue loaded structure a small non critical defect may grow to a larger defect with a critical size due to the service load. Therefore, crack growth estimation is essential for a fitness for purpose assessment of fatigue loaded structures. The crack growth estimation may show that a repair can be postponed to a more suitable time or even show that the defect will not become critical during the service life (This may be due to the fact that the defect is in or growing into a low stressed area).
This paper deals with the fatigue crack growth part of the fitness for purpose assessment. A brief summary of a guideline drawn up in the Netherlands [1] is given. The various parts of a fatigue assessment will be highlighted, such as: defect schematization and recategorization (see section 2), crack growth laws and their constants (see section 3), stress intensity factors (see section 4) and a calculation procedure (see section 5).
The paper ends with conclusions and recommendations for further research (section 6).
Sections 2,3,4 and 5 are mainly based on a study carried out by TNO (Netherlands Organisation for Applied Scientific Research) within the framework of a NIL (Nederlands Instituut voor Lastechniek) and CS (Centrum Staal) research project [1, 2, 3 and 4].

2. DEFECT SCHEMATIZATION

2.1. Idealization of defects

The size and the location of the defect is normally determined by non destructive testing. The actual measured dimensions can be irregular and not suited for a crack growth calculation procedure. In general a fatigue crack will tend to grow to an idealized shape. Therefore an idealization of the measured dimensions is allowed.
Three types of planar flaws can be considered:
- Through flaws   idealization: rectangle   width   2a
- Surface flaws   : semi-ellipse depth a, width 2c
- Embedded flaws   : ellipse   minor axis a and major axis c
Their dimensions (a and c) are determined from the height and the length of their containment rectangles (see table 1). The plane in which the idealized flaw is located is perpendicular to the stress that is used for the calculation of the fatigue crack extension. The actual flaw should be projected to that plane and then be idealized. This idealization procedure is in accordance with other guidelines [5 and 6].

type of flaw	actual flaw	idealization
through flaw		
surface breaking flaw		
embedded flaw		

Table 1 Idealization of flaws

2.2 Interaction of defects

During the fatigue crack growth, interaction of two ore more defects can occur. This is often the case at weld toes, where multiple crack initiation followed by coalescence and crack growth at low aspect ratios occurs. Interaction between a defect and a free surface is also possible.

Existing interaction criteria [5 and 6] are developed for the assessment of instable (brittle) fracture and are not suitable for fatigue crack growth (see [20]). Therefore a new set of interaction criteria is proposed [4].

In general, interaction is considered if the distance of two flaws, in relation to the dimensions of these flaws, is smaller than a given value or zero. When this criterion is met the two flaws have to be considered as one single flaw with the idealization rules given in 2.1. Table 2 gives the new fatigue interaction criteria for through flaws, surface flaws and embedded flaws. Mutual interaction and interaction with a free surface is considered.

When interaction occurs during the fatigue crack growth, the calculation is resumed after recategorization, starting with the new idealized crack dimensions.

3. CRACK GROWTH MODELS AND CONSTANTS.

3.1. Crack growth models.

Fatigue crack growth models for welded structures, based on linear elastic fracture mechanics have been described recently by several authors [7, 8, 9, 10, 11, 12 and 14]. In general, the crack growth model gives the relation between the crack growth rate (da/dN) and the fatigue loading parameter (stress intensity factor range (ΔK)). This relation, called the Paris-Erdogan relation is as follows (see region II in figure 1) :
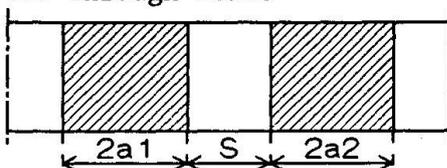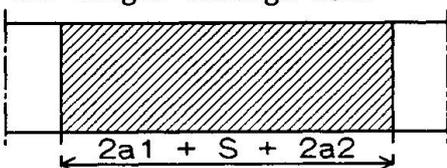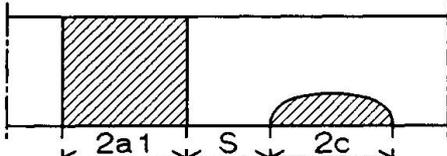
interacting flaws and surfaces	criteria	recategorized flaw
two through flaws $2a1$ — S — $2a2$	$a_1 < a_2$ and $S < 2a_1$	one single through flaw $2a1 + S + 2a2$
through flaw and surface flaw $2a1$ — S — $2c$	$S < 2a_1$ and $S < 2c$	one single through flaw $2a1 + S + 2c$
through flaw and embedded flaw $2a1$ — S — $2c$	$S < 2a_1$ and $S < 2c$	one single through flaw $2a1 + S + 2c$
surface flaw and opposite surface $T-a$ $2c$	$T-a = 0$	one single through flaw $2c$
two surface flaws $2c1$ — S — $2c2$	$S = 0$	one single surface flaw $2c1 + 2c2$
surface flaw and embedded flaw S	$S = 0$	one single surface flaw
embedded flaw and free surface p	$p = 0$	one single surface flaw
two embedded flaws S	$S = 0$	one single embedded flaw
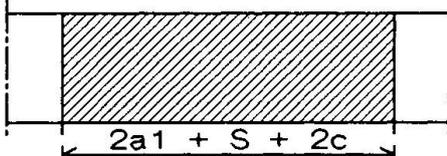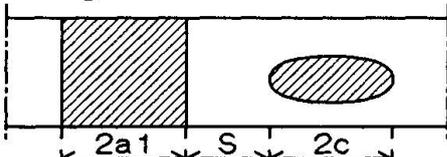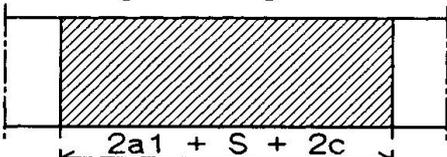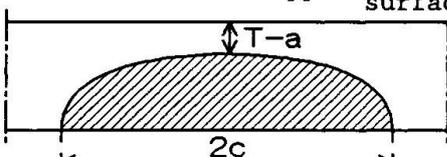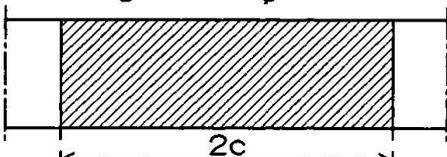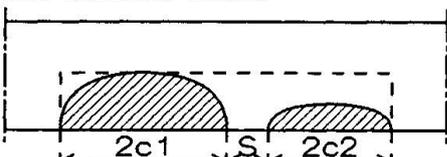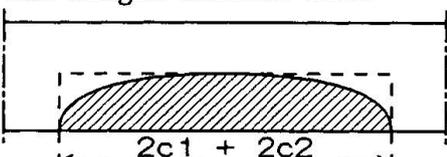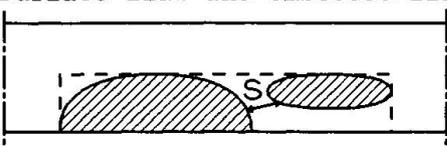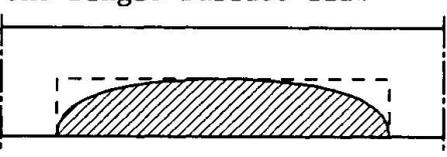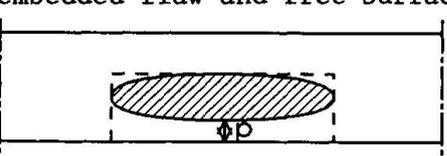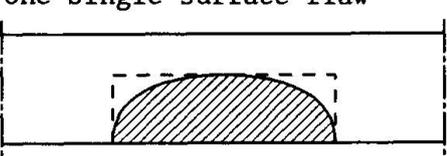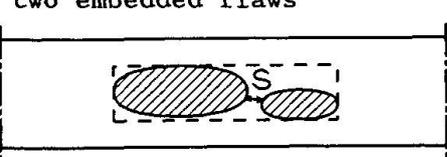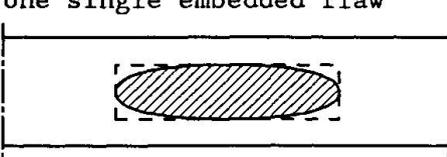
Table 2 Interaction of coplanar flaws during fatigue crack growth.

$$da/dN = C \ (\Delta K)^m \qquad (1)$$

where C and m are crack propagation constants.

In the near threshold range (region I) the influence of the threshold value of ΔK (ΔK_{th}) can also be incorporated in the relation:

$$da/dN = C \ (\Delta K^m - \Delta K_{th}^m) \qquad (2)$$

In the upswing of the crack growth curve (region III) the influence of the critical value of K (K_c), combined with the load ratio R ($=F_{min}/F_{max}$) can be taken into account.

$$da/dN = \frac{C \ (\Delta K)^m}{(1-R)K_c - \Delta K} \qquad (3)$$

Fig 1 gives a general view of the da/dN-ΔK curve and the validity of the three crack growth relations mentioned above.

3.2. Crack propagation constants

The crack growth constants C and m, and ΔK_{th} have to be determined for the relevant material and conditions (environment, frequency, etc). Figure 2 shows an experimental crack growth curve of an Fe E 355-KT material used in an ECSC-SMOZ project [12]
When no specific data are available the following values can be used for ferritic steels with a proof stress below 600 N/mm2 operating in air or other non aggressive environments at temperatures up to 100 °C:

m = 3

$$C = 3 \ 10^{-13} \ \text{(units N and mm)} \qquad (4)$$

For marine environment and normal wave frequency ($\approx$ 0.1 Hz) C becomes:

$$C = 2.3 \ 10^{-12} \ \text{(units N and mm)} \qquad (5)$$

Fig. 1 Crack growth rate curve.

C = 1.105E-13 (N,mm)
m = 3.081

SIF range [N/mm3/2]
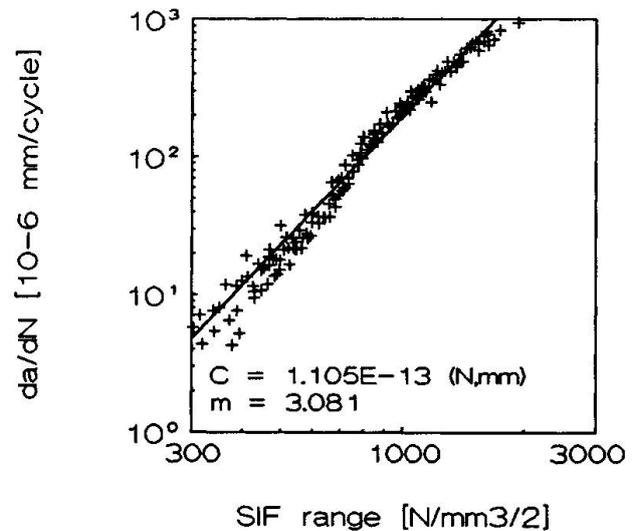
Fig. 2 Experimental da/dN-ΔK curve.

The values of (4) and (5) are a safe upperbound of the crack growth data.
For as-welded structures the following threshold value of ΔK should be used:

$$\Delta K_{th} = 63 \ N/mm^{3/2} \qquad (6)$$

4. STRESS INTENSITY FACTORS

4.1. Governing stresses.

The stress intensity factor (SIF,K) range is the difference between the maximum SIF and the minimum SIF during a load cycle. The SIF is a measure for the magnitude of the stresses near the crack tip; eqn. (7).

$$K = Y \, \sigma \, \sqrt{(\pi a)} \qquad\qquad\qquad (7)$$

where: σ - remotely applied stress
       Y   - correction factor depending on geometry and loading conditions
       a   - crack depth

The stress variations for a fatigue crack growth calculation have to be determined from the complete load history during the (remaining part of the) service life or from the expected load history to the next inspection.
The stresses in a welded detail can be separated in (see figure 3):
a) Membrane stresses (σ_m), being the average nominal stress across the section thickness due to the applied load on the section.
b) Bending stress (σ_b), being the bending part of the nominal stress across the section thickness due to the applied load on the section.
c) Residual stress (σ_r) across the section thickness. These stresses are self-equilibrating. σ_r is often due to the welding or fabrication process of the detail.
d) Peak stress (σ_p) due to local discontinuities (such as: weld toes, etc.).
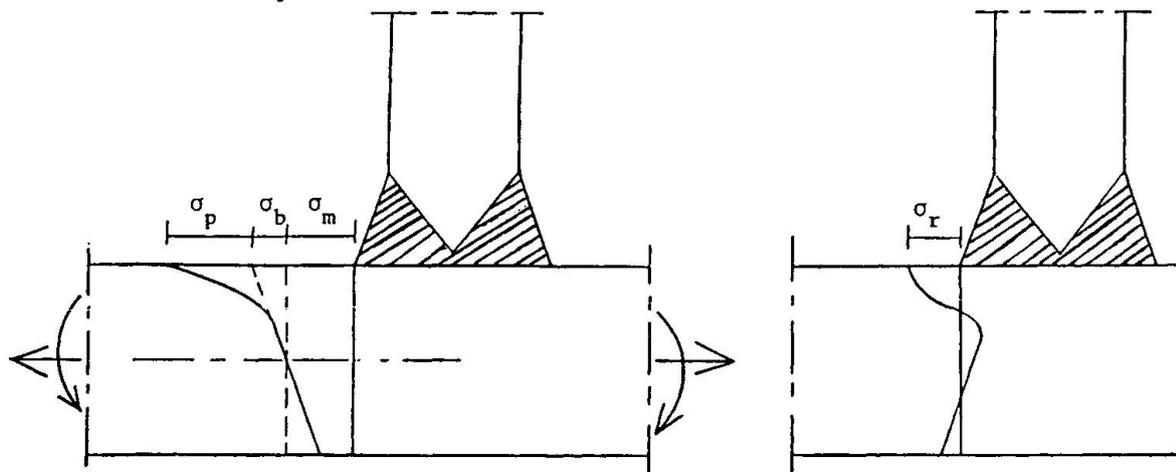
Fig. 3 Stresses in a welded detail.

The governing fatigue stresses for an as-welded structure are the elastic stress ranges of σ_m and σ_b at the crack location for the uncracked geometry. The effect of the global geometry should be incorporated in the stress analysis, while the effect of the local geometry (weld shape, etc.; causing σ_p) should be excluded. This effect of the local geometry will be incorporated in the determination of the stress intensity factor by the stress intensity concentration factor (M_k). For as welded structures the mean stress level has no influence on the fatigue crack growth. The residual stress level at the weld toe in as welded structures generally approaches the tensile yield stress. This implies that the stress range is always fluctuating from tensile yield stress downwards and the complete stress range is effective for crack growth.
For stress-relieved structures loaded with a fatigue load with a negative R ($-\sigma_{min}/\sigma_{max}$)ratio, the complete stress range may not be effective. However due to settlements or assembling stresses the actual stress level may differ from the calculated one. Therefore it is recommended for steel structures not to use the possible beneficial effect due to stress relieving. For special structures

where the value of the mean stress is known (e.g. a complete stress relieved structure) the beneficial effect of a low mean stress level may be used.
In case of a random load sequence a counting procedure (such as rainflow counting) may be used to determine the governing stress ranges.
The stress range perpendicular to the crack surface (mode I stress range) is the governing stress range in complex stress situations (e.g. biaxial stresses).

4.2. SIF in 2-D geometries

The SIF of a constant depth edge crack in a welded 2D geometry (see fig. 4) is generally given as follows:

$$K = [M_{k,m} \; M_m \; \sigma_m + M_{k,b} \; M_b \; \sigma_b] \; \sqrt{(\pi a)} \tag{8}$$

where: M_k - stress intensity concentration factor for the influence of the weld geometry
  M - stress intensity correction factor for the strip without the weld geometry
  m and b as index means for membrane stress and for bending stress respectively.

M is a function of the relative crack depth (a/T). Formulas can be found in literature [1, 9 and 13].
M_k is a function of a/T , the weld dimensions (see fig. 4) and the weld type. Assuming no interaction between the influence of the relative weld width (L/T), the weld angle (θ) and the relative weld toe radius (ρ/T) the following formula for M_k can be written.

$$M_k = f_L(a/T,L/T) \cdot f_\theta(a/T,\theta) \cdot f_\rho(a/T,\rho/T) \tag{9}$$

where: f_L - a correction factor for the influence of the relative weld width (L/T) for a specific weld type with a certain weld angle and weld toe radius.
  f_θ - a correction factor for the influence of the weld angle (θ).
  f_ρ - a correction factor for the influence of the relative weld toe radius (ρ/T).
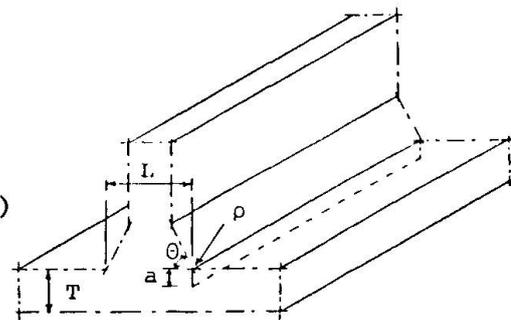
Fig. 4 Constant depth crack.

A powerful tool to determine SIFs and M_k values of weld geometries is the finite element method (FEM) [9 , 14 and 18].
Smith and Hurworth [15] and Maddox et al. [16] have determined M_k values with a FEM technique for butt welds and T-and X-joint geometries (see fig. 5). For butt welds and X-joints a set of formulas for M_k values was derived by Maddox et al. [16]. These formulas are valid for weld toe angle θ - 45° and weld toe radius ρ - 0. The formulas are functions of the relative crack depth (a/T) and relative weld width (L/T).

$$M_k = f_L(a/T,L/T) \tag{10}$$

The functions f_L and the range of applicability can be found in [5, 14 and 16]
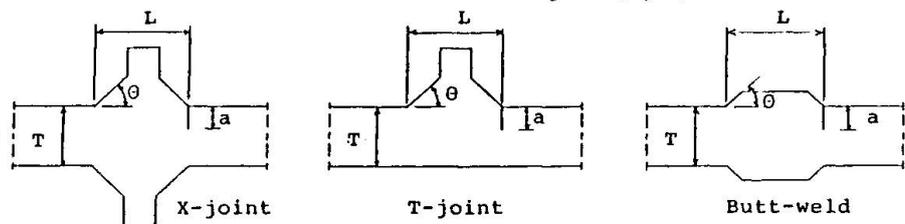
Fig. 5 Geometries studied by Smith and Hurworth [15] and Maddox et al. [16].

Dijkstra et al. [14] determined M_k values for T-joint geometries (see fig 6). A formula (eqn. 11) was developed for geometries with θ - 70° and ρ - 0.

$$M_k - A + \frac{B}{a/T-C} \qquad (11)$$

The values of A, B, and C are given in
table 3.
The influence of the relative weld toe
radius was also expressed in a formula
(eqn 12).
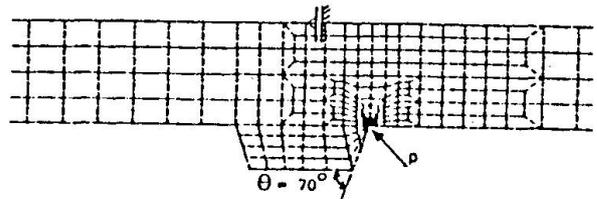
Fig 6. Finite element mesh of T-joint.

$$f_\rho - 1 - A_\rho . e^{-B_\rho . a/T} \quad \text{for} \quad a/T \le 0.1 \quad (12) \quad \text{and} \quad f_\rho - 1 \quad \text{for } a/T > 0.1 \quad (13)$$

where: $A_\rho - A_{\rho 1} + A_{\rho 2}/(\rho/T - A_{\rho 3})$ (14) and $B_\rho - B_{\rho 1} + B_{\rho 2}.(\rho/T)^2$ (15)

See table 4 for the coefficients $A_{\rho 1}$ to $B_{\rho 2}$ (applicability $.00714 \le (\rho/T) \le .125$).

So the M_k value for a T-joint with $\theta - 70°$ and a relative weld toe radius
$0.00714 \le (\rho/T) \le 0.125$ can be determined as follows:

$$M_k - [A + B/(a/T-C)].f_\rho \qquad (16)$$

where: A, B, and C are the values given in table 3.
f_ρ is the function of eqn. (12 to 15)

Based on the information given by Smith and Hurworth [15] Dijkstra et al. [14]
developed a formula for f_θ with $\theta = 45°$ as reference value:

$$f_\theta - (10.a/T)^{-\frac{1}{2}\log A_\theta} \quad \text{for } 0.001 \le a/T \le 0.1 \qquad (17)$$

where: $A_\theta - 13.096 \cdot 10^{-3} + 28.119 \cdot 10^{-3}\theta - 139.45 \cdot 10^{-6}\theta^2$ (18)

$$f_\theta - 1 \qquad \text{for } a/T > 0.1 \qquad (19)$$

The range of application of eqns. (17 to 19) is: $25° \le \theta \le 65°$.

With the information given in this section one can determine the SIF of a welded
T- or X-joint taking the influence of L/T, ρ/T and θ into account for a 2-D
geometry.

region	load case	A	B	C
I	b	1.1362	0.015011	-0.0034398
$0 \le a/T < 0.025$	m	1.0291	0.012040	-0.0034689
II	b	0.88539	0.031426	-0.015361
$0.025 \le a/T < 0.1$	m	0.93832	0.016203	-0.0065430
III	b	0.95471	0.019388	0.0047441
$0.1 \le a/T < 0.4$	m	0.96858	0.011363	0.0044927

Table 3   Curve fitting coefficients for Mks at weld
toes in T-joints with $\theta = 70°$ and $\rho - 0$.

loading	$A_{\rho 1}$	$A_{\rho 2}$	$A_{\rho 3}$	$B_{\rho 1}$	$B_{\rho 2}$
bending	0.70754	-0.020160	-0.024502	75.323	-1541.7
membrane	0.71032	-0.024015	-0.028061	105.29	-1993.8

Table 4   Curve fitting coefficients for f_ρ.

4.3 SIF in 3-D geometries.

The SIF of a semi-elliptical crack at a weld toe in a 3D geometry can be
expressed in the crack depth (a) direction and in the crack width (c) direction
(see fig. 7) as follows:

$$K_a = [M_{k,m,a} \ M_{m,a} \ \sigma_m + M_{k,b,a} \ M_{b,a} \ \sigma_b]\sqrt{(\pi a)}/\Phi \qquad (20a)$$

$$K_c - [M_{k,m,c} \ M_{m,c} \ \sigma_m + M_{k,b,c} \ M_{b,c} \ \sigma_b]\sqrt{(\pi a)}/\Phi \qquad (20b)$$

where: a and c as index means for crack depth and for crack width direction
        respectively.
        Φ - elliptical integral of the second kind,
                        approximation $\Phi - [1 + 1.464 \ (a/c)^{1.65}]^{0.5}$
        for other symbols see equation (8)

The correction factors for the flat plate ($M_{m,a}$, $M_{b,a}$, $M_{m,c}$ and $M_{b,c}$) presented
by Newman and Raju [17] can be used.
The 3-D SIF can also be determined
with FEM. Van Straalen et al. [18]
determined SIFs for a T-plate with a
weld discontinuity. The geometry and
the finite element model are given in
fig. 8 and 9. SIFs were calculated for
four crack geometries. The most
important results are given in table
5. More results are given in [18 and
14]. For comparison the M_k values for
a similar 2D geometry have also been
tabulated. The 2D M_k values are higher
than the 3D M_k values. This can be
explained by the stiffening effect
of the stub in the uncracked part of
the plate in the 3D geometry. The
ratio (ω) of $M_{k,3D}$ and $M_{k,2D}$ is also given in table 5. This ratio can be seen as
a reduction factor for the application of 2D M_k values in a 3D geometry. Due to
the limited amount of data no general expression of this reduction factor can be
given.

Fig 7 Semi-elliptical crack at the weld
                                        toe.

Comparison of the calculated SIF with experimental crack growth data showed a
lower crack growth rate than predicted with the theoretical SIF for the geometry
of fig 8 and 9 [12].

| loadcase | direction | crack | | M_k | | ratio |
		depth a [mm]	width c [mm]	3D	2D	$\dfrac{M_{k,3D}}{M_{k,2D}}$ ω
membrane	depth a	6.49	10.14	0.964	1.041	0.926
		8.95	15.80	0.930	1.020	0.912
		11.85	25.90	0.920	1.008	0.913
		16.00	40.70	0.926	1.000	0.927
membrane	width c	6.49	10.14	1.260	1.498	0.841
		8.95	15.80	1.234	1.498	0.824
		11.85	25.90	1.166	1.498	0.778
		16.00	40.70	1.225	1.498	0.818
bending	depth a	6.49	10.14	0.986	1.078	0.915
		8.95	15.80	0.926	1.043	0.888
		11.85	25.90	0.899	1.021	0.872
		16.00	40.70	0.895	1.000	0.895
bending	width c	6.49	10.14	1.353	1.650	0.820
		8.95	15.80	1.325	1.650	0.803
		11.85	25.90	1.286	1.650	0.779
		16.00	40.70	1.324	1.650	0.802

Table 5   SIF and M_k for geometry D-2-2
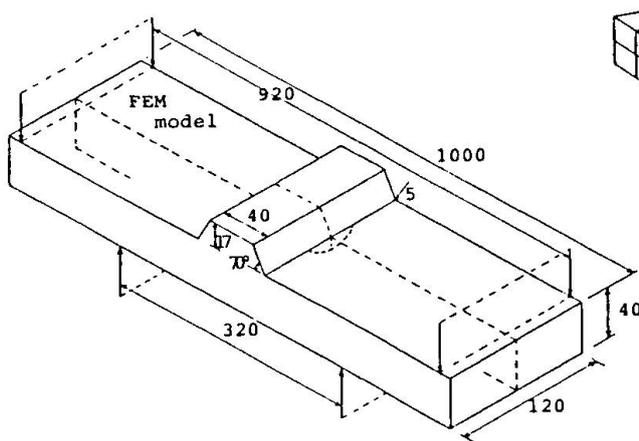
Fig 8. Dimensions of 3-D specimen
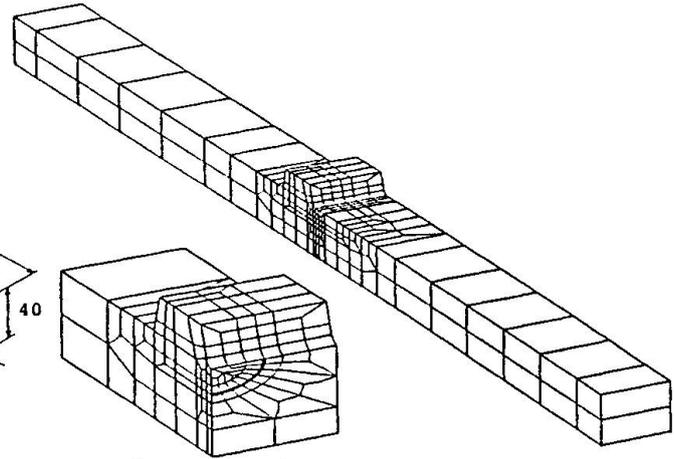
Fig 9. Mesh of 3-D specimen.

5   CALCULATION PROCEDURE.

The lifetime can be calculated by integrating the crack growth law from the initial defect size (a_i) to the final (allowable) defect size (a_f). The integration can be done either analytically or numerically. Due to the complex relation between ΔK and a the analytical integration of the crack growth law is an impractical procedure. Therefore a numerical (step by step) calculation procedure carried out by a computer is recommended.

TNO-IBBC has developed the program FAFRAM (FAtigue FRActure Mechanics) [19]. As the governing parameter for the calculation a crack extension (Δa) relative to the existing crack depth (a) was chosen. In order to get acceptable accuracy relatively small values should be taken for Δa (Crack extensions Δa of 5% of the present crack size give in general acceptable results). The numerical procedure will be illustrated for the semi-elliptical crack of figure 7. Assuming only bending stresses $(\Delta\sigma)$ the expressions for ΔK_a and ΔK_c can be simplified to:

$$\Delta K_a = f_a \cdot \Delta\sigma \sqrt{\pi a} \tag{21a}$$

$$\Delta K_c = f_c \cdot \Delta\sigma \sqrt{\pi a} \tag{21b}$$

$$\text{where:} f_a = \frac{M_{k,b,a} \cdot M_{b,a}}{\Phi} \tag{22a}$$

$$f_c = \frac{M_{k,b,c} \cdot M_{b,c}}{\Phi} \tag{22b}$$

The procedure is as follows (see table 6 as a way of presenting the results):

1. With the actual crack depth (a_i) and half crack width (c_i) and the other geometrical parameters the values for f_a and f_c can be calculated.
2. Using the stress range $(\Delta\sigma)$ the SIFs for crack depth (ΔK_a) and crack width (ΔK_c) can be calculated with equation (21).
3. Assuming a crack extension Δa the corresponding number of cycles can be calculated with the Paris relation.

$$\frac{\Delta a}{\Delta N} = C (\Delta K_a)^m \qquad \text{or:} \qquad \Delta N = \frac{\Delta a}{C (\Delta K_a)^m} \tag{23}$$

4. The crack extension in the width direction can also be calculated with the Paris relation.

$$\frac{\Delta c}{\Delta N} = C (\Delta K_c)^m \qquad \text{or:} \qquad \Delta c = \Delta N C (\Delta K_c)^m = \Delta a \left(\frac{\Delta K_c}{\Delta K_a}\right)^m \tag{24}$$

5.The number of cycles has to be increased with ΔN.

$$N_{i+1} = N_i + \Delta N \qquad (25)$$

6.The crack dimensions have to be increased with the crack extensions:

$$a_{i+1} = a_i + \Delta a \qquad \text{and:} \qquad c_{i+1} = c_i + \Delta c \qquad (26)$$

7.With the new crack dimensions (a_{i+1}, c_{i+1}) the next step can be calculated, starting with point 1 above.

8.The calculation has to be continued until the allowable crack depth (a_f) or until the required number of cycles (N_{req}).

9.The calculated number of cycles or crack size has to be assessed at its acceptability.

For 2D geometries the calculation has to be carried out in the a-direction only.

crack dimensions		a-direction			c-direction			number of cycles		
depth a [mm]	width c [mm]	f_a [-]	ΔK_{a} [N/mm$^{1.5}$]	Δa [mm]	f_c [-]	ΔK_{c} [N/mm$^{1.5}$]	Δc [mm]	N_i [-]	ΔN [-]	N_{i+1} [-]
0.25	0.25	2.177	196.12	0.025	2.901	270.19	0.065	0	33141	33141
0.28	0.32	2.242	217.60	0.028	2.929	285.14	0.062	33141	26692	59834
a_i $a_i + \Delta a$	c_i $c_i + \Delta c$	f_{a_i}	ΔK_{a_i}	Δa	f_{c_i}	ΔK_{c_i}	Δc	N_i	ΔN	$N_i + \Delta N$

Table 6. Calculation of crack growth

More results of crack growth calculations can be found in earlier papers and reports [8, 9, 12, 14 and 20]. The effect of several parameters are demonstrated in these publications.

6 CONCLUDING REMARKS AND RECOMMENDATIONS

-With the information in the paper and the references given to open literature a fatigue crack growth calculation of a defective welded joint can be carried out.

-The recategorization rules for interacting fatigue cracks given in this paper are less conservative than existing rules (Existing rules are developed for instable (brittle) fracture).

-The Paris-Erdogan relation can be applied in most cases as the crack growth law.

-Stress intensity factors for 2-D weld geometries are given.

-The influence of the weld on the stress intensity factor (SIF) is smaller for a 3-D geometry (semi-elliptical crack) than for a 2-D geometry (constant depth crack). However the information of 3-D SIF is limited. Therefore it is recommended to generate more information for 3-D cracks.

-Experimental crack growth data for 3-D geometries is needed to validate the crack growth model for a 3-D situation.

-A fatigue crack growth calculation procedure suitable for a computer program is given.

REFERENCES

1. DIJKSTRA, O.D., SNIJDER, H.H. and RONGEN, H.J.M. van., Fitness for purpose assessment of fatigue loaded welded joints in steel structures. IBBC-TNO report BI-87-110/63.4.5700 March 1989.

2. SNIJDER, H.H. and DIJKSTRA, O.D., Stress intensity factors for cracks in welded structures and containment systems. IBBC-TNO report BI-88-128/ 63.4.5700, August 1988.
3. DIJKSTRA, O.D. and SNIJDER, H.H., Fatigue crack growth models and their constants. IBBC-TNO report BI-88-027/63.4.5700, February 1989.
4. RONGEN, H.J.M. van., Categorization and interaction of fatigue cracks. MI-TNO report 89M/02316/ROH, February 1989.
5. IIW recommendation on "The Application of an Engineering Critical Assessment in Design, Fabrication on Inspection to assess the Fitness for Purpose of Welded Products", Part 4, Fatigue, IIW document V-878-88/X-1167-88/XIII-1283-88/XV-665-88.
6. British Standards Institution "Guidance on some methods for the derivation of Acceptance levels for defects in fusion welded joints", PD6493; 1980, London.
7. BELL, R., VOSIKOVSKY, O., BURNS, D.J., MOHAUPT, U.H., A Fracture Mechanics Model for Life Prediction of Welded Plate Joints. Steel in Marine Structures, edited by C. Noordhoek and J. de Back, Elsevier, pp 901-910, 1987.
8. DELFT, D.R.V. van, DIJKSTRA, O.D., and SNIJDER, H.H.,The Calculation of Fatigue Crack Growth in Welded Tubular Joints Using Fracture Mechanics. 18th Offshore Technology Conference, OTC 5352, Houston, 1985.
9. DIJKSTRA, O.D., SNIJDER, H.H., OVERBEEKE, J.L., WILDSCHUT,H., Prediction of Fatigue Crack Growth for Welded Joints Using Stress Intensity Factors Determined by FEM Calculations. Steel in Marine Structures, edited by C.Noordhoek and J. de Back, Elsevier, pp 885-899, 1987.
10.THORPE, T.W., A Simple Model of Fatigue Crack Growth in Welded Joints. Department of Energy, Offshore Technology Report, OTH 86 225, Her Majesty's Stationery Office, 1986, London.
11.VOSIKOVSKY, O., BELL, R., BURNS, D.J., MOHAUPT, U.H., Fracture Mechanics Assessment of Fatigue Life of Welded Plate T-Joints Including Thickness Effect. Behaviour of Offshore Structures, Elsevier, Amsterdam, 1985.
12.DIJKSTRA, O.D., SNIJDER, H.H., OVERBEEKE, J.L., WILDSCHUT, H. and SCHOLTE, H.G. Fatigue behaviour of welded joints in offshore structures. ECSC convention 7210-KG/602(F7.5/84) Delft, December 1988.
13.ROOKE, D.P. and CARTWRIGHT, D.J., Compendium of Stress Intensity Factors.London, Her Majesty's Stationary Office, 1976.
14.DIJKSTRA, O.D., SNIJDER, H.H. and STRAALEN IJ.J., Fatigue crack growth calculations using stress intensity factors for weld toe geometries. OMAE conference, The Hague, March 1989.
15.SMITH, I.J. and HURWORTH, S.J., The effect of geometry changes upon the predicted fatigue strength of welded joints. The Welding Institute Report 7819.01/84/394.3, Cambridge, 1984.
16.MADDOX, S.J., LECHOCKI, J.P., ANDREWS, R.M., Fatigue analysis for the revision of PD 6493: 1980'The Welding Institute Report 3873/1/86, Cambridge, 1986.
17.NEWMAN, J.C., and RAJU, I.S., Stress intensity factor equations for cracks in three-dimensional finite bodies subjected to tension and bending loads. NASA TM 85793, Langley Research Center, Virginia, 1984.
18.STRAALEN, IJ.J. van, DIJKSTRA, O.D. and SNIJDER,H.H., Finite element calculations to obtain stress intensity factors of semi-elliptical surface cracks in a finite width plate with stub and without stub - Calculations with DIANA for specimen D-2-2 of the SMOZ fracture mechanics programme, Report no. BI-88-015/63.8.0310 and BI-88-133/63.5.5860-310, TNO-IBBC, Rijswijk, The Netherlands,1988.
19.SNIJDER, H.H. and DIJKSTRA, O.D., FAFRAM - Computer program for the evaluation of FAtigue behaviour of structures using FRActure Mechanics. TNO-IBBC report BI-85-102, Rijswijk, 1985.
20.SNIJDER, H.H., DELFT, D.R.V. van, DIJKSTRA, O.D., and NOORDHOEK, C., Fatigue crack growth modelling for multiple initiated cracks at weld toes in tubular joints. BOSS conference June 1988, Trondheim.

An Alternative to Miner's Rule for Cumulative Damage Calculations?

Une alternative à la loi de Miner pour calculer le cumul du dommage?

Eine Alternative zur Miner'schen Regel für die Berechnung der Schadens-Akkumulation?

Tim GURNEY
Chief Research Engineer
The Welding Institute
Cambridge, England

Tim Gurney, born 1929, read Mechanical Sciences at Cambridge University where subsequently, he also obtained his PhD. Following four years with a firm of Consulting Engineers, he joined The Welding Institute, where he has worked primarily on fatigue of welded structures.

Stephen MADDOX
Principal Fatigue Consultant
The Welding Institute
Cambridge, England

Apart from three years' industrial consultancy at Southampton University, Stephen Maddox has been with The Welding Institute since graduating in Civil Engineering in 1966. His research field is fatigue of welded structures, including design recommendations and the application of fracture mechanics, for which he received his PhD.

SUMMARY

Based upon an analysis of the available variable amplitude fatigue test results for welded joints, it is shown that, in some circumstances, Miner's rule may be unsafe and that the Area rule may be a better alternative. This applied particularly for short block length loading and wide band loading. However, further work is required to confirm these findings.

RÉSUMÉ

Sur la base d'une analyse des résultats d'essais de fatigue à amplitude variable sur des joints soudés, on peut montrer que, dans certains cas, la loi de Miner n'est pas du côté de la sécurité, et que la «règle des surfaces» serait une meilleure alternative. Ceci s'applique en particulier quand la contrainte maximum se produit fréquemment et pour des chargements à bande étendue. Cependant, des études supplémentaires doivent être faites pour confirmer ces conclusions.

ZUSAMMENFASSUNG

Basierend auf einer Analyse der erhältlichen Versuchsresultate zur Ermüdung von Schweissverbindungen unter variabler Amplitude wird gezeigt, dass unter gewissen Umständen die Miner-Regel auf der unsicheren Seite liegt und deshalb die Anwendung der «Oberflächen-Regel» angebracht erscheint. Dies trifft besonders auf «short block length-» und «wide band loading»-Spektren zu. Um diese Beobachtungen zu bestätigen, sind jedoch weitere Forschungsarbeiten unabdingbar.

1. INTRODUCTION

In service, the great majority of structures which are liable to suffer fatigue failure are subjected to variable amplitude loading. For historical reasons, however, and particularly on account of the capabilities of fatigue testing machines, most of the experimental data, certainly for welded joints, has been obtained under constant amplitude loading. The assessment of the fatigue life of structures therefore requires the use of some sort of cumulative damage rule and Miner's [1] linear damage rule is the one most commonly used.

As far as is known, the first time that this rule appeared in a Standard for the design of welded joints was in 1962 when it was introduced into BS 153, Steel Girder Bridges. At that time such an action was probably quite unjustified; it was really a simple 'act of faith'. After all, Miner had originally proposed his rule for defining the life to crack initiation of unnotched specimens of aluminium alloy. There were no sound reasons for assuming that it would be equally applicable to the life to rupture of severely notched members in steel, where it was known that the great majority of the life consisted of crack propagation. It was only much later that it was shown by Maddox [2] that Miner's rule could be derived by fracture mechanics for any specimen/joint involving crack propagation to failure. Since then, however, Miner's rule, or a simpli- rule based on Miner's rule, has appeared in several National Standards.

The obvious problem is, "Is it right?" In order to try to answer that question an extensive literature survey has recently been carried out to gather together and analyse all the available test results for welded steel specimens subjected to variable amplitude loading, either of the programmed or random variety, in air. This included recalculating the values of $\Sigma\frac{n}{N}$ for every test specimen so as to ensure that all the results were defined in the same manner; unbroken specimens were ignored.

It was found that numerous test series gave mean values, and particularly lower limit values, of $\Sigma\frac{n}{N}$ which were less than 1.0. This has sometimes been taken as proof that Miner's rule is unsafe. However, that is not necessarily true, since one could reasonably expect the scatter in variable amplitude test results to mirror that found in constant amplitude results. In other words, if a specimen would have given a low life under constant amplitude loading, it seems reason- able to assume that it would also be expected to give a low life under variable amplitude loading. Furthermore, to a first approximation, it also seems reason- able to assume that the amount of scatter would be the same with the two differ- ent types of loading.

Although no detailed analysis has been made of the scatter in constant amplitude results, inspection of a number selected at random suggests that in a single S-N curve the overall scatter can be represented by a factor of between 2 and 3 on life. For comparison Haibach [3] proposed that his 'standard curve' should have corresponding factors of 3 at 10^5 and 4 at 10^6 cycles.

For a factor of 2.0 the corresponding expected range of values of $\Sigma\frac{n}{N}$ becomes about 0.7 - 1.4, while for a factor of 3.0 it is about 0.6 - 1.8. Thus any values of $\Sigma\frac{n}{N}$ greater than about 0.6 - 0.7 can reasonably be regarded as normal, provided that in a test series there are also some corresponding 'high' values. Thus, for Miner's rule to be proved safe one should expect a series of variable amplitude fatigue tests to give a mean value of $\Sigma\frac{n}{N}$ approximately equal to 1.0 (or more) but with individual results down to about 0.6. In fact it was found that many test series gave values which were considerably lower, thereby sug- gesting that Miner's rule certainly is not safe under all conditions.

Fig. 1 shows the same data expressed in terms of the 1292 individual test results. The values extend from 0.16 to 9.12 but it should be noted that three test series for which the mean values of $\Sigma\frac{n}{N}$ were in the range 12.3 - 15.7 have been ignored. These were so out of line with the other results that it was assumed that some error must have occurred in reporting the results. Results
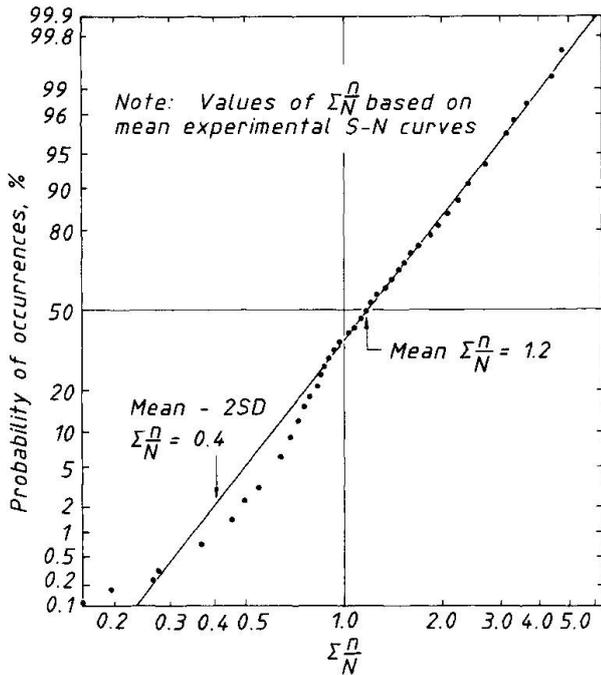
Fig.1 Summary of published values of $\Sigma\frac{n}{N}$

obtained using spectra in which all cycles pulsated downwards from a constant maximum stress have also been omitted. As before, the results are based upon the corresponding mean experimental S-N curve extrapolated linearly downwards.

Although the individual values of $\Sigma\frac{n}{N}$ varied widely, the mean and mean minus 2 standard deviations (SD) values were approximately 1.2 and 0.4 respectively. It is therefore tempting to argue that Miner's rule, with $\Sigma\frac{n}{N} = 1.0$, is a satisfactory design approach, since the low value of 0.4 is counterbalanced by the fact that design is normally based upon the mean minus 2 SD design curve and not the mean curve. In the British design rules the difference in life between the two curves, represented by the ratio $\dfrac{\text{mean} - 2 \text{ SD life}}{\text{mean life}}$ at any given stress, is as follows:

Class	D	E	F	F2	G
Ratio of lives	0.381	0.315	0.366	0.350	0.437

Thus, in all cases except Class G, the reduction in life between the two curves is more than 0.4 so that, basing the calculation on the mean minus 2 SD curve would be safe for more than 97.7% of situations.

This is, however, a fallacious approach. The reduction in life between the mean and mean - 2 SD design curve only takes account of the scatter found in constant amplitude tests, caused by such variables as differences in local joint geometry. It does not allow for any extra variability in life, if such exists, due to variable (rather than constant) amplitude loading. It is therefore necessary to consider the influence of the type of loading separately and not to assume that it is necessarily covered by using the mean - 2 SD design curve.

2. INFLUENCE OF TYPE OF LOADING ON FATIGUE LIFE

The following information about the influence of the type of loading on the value of $\Sigma\frac{n}{N}$ is based heavily on the results of work at The Welding Institute [4,5] over the last six or seven years. All the work involved longitudinal non-load-carrying fillet welds, either on the edge or surface of the stressed plate, because of the known tendency of such joints to give very little scatter; it was therefore hoped that it would be easier to define any trends which might emerge. It is convenient to consider the results more or less in chronological order.
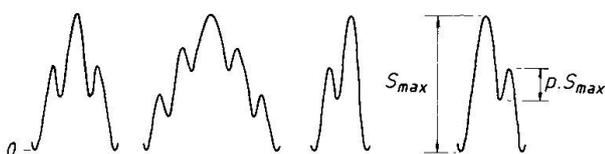

Fig.2 Typical loading in initial tests

The initial tests [4] were carried out with very simple stress histories, consisting essentially of constant amplitude loading with one or more excursions applied on each stress cycle (Fig. 2). With this type of loading there are few real problems
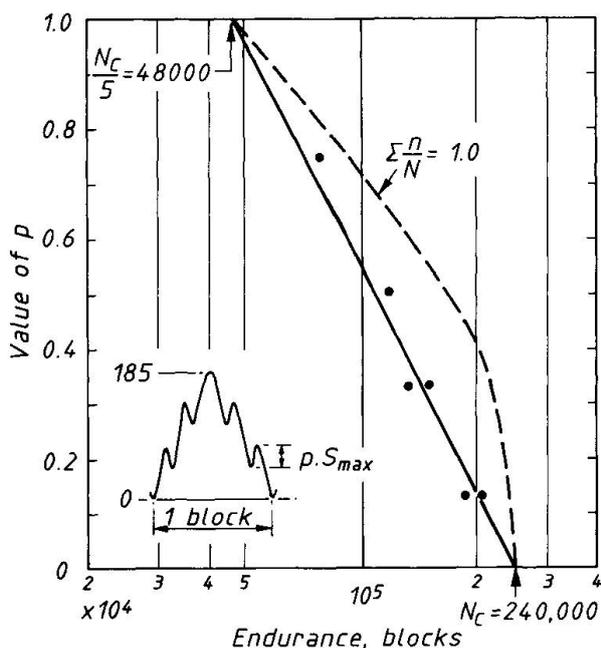
Fig.3 Typical results obtained using
      simple stress sequences

with stress counting, although in all cases the reservoir method was used. On the other hand there is certainly a potential stress interaction problem and the expectation was that the tensile peak of the main constant amplitude cycle would tend to introduce compressive residual stresses at the crack tip and thereby make the smaller cycles less damaging. As a result of this stress interaction it was anticipated that the life would always be greater than that predicted by Miner's rule – in other words it was expected that $\Sigma\frac{n}{N}$ would be greater than 1.0. In fact the opposite was found to be true.

A typical set of results is shown in Fig. 3. They relate to specimens tested under a main constant amplitude cycle of 185 N/mm^2 at R = 0 with four subsidiary cycles of magnitude p. In this context p represents the ratio between the stress range of the excursions and of the main cycle. Thus, using this nomenclature, p can clearly vary from 0 to 1.0 and at the two extremes (p = 0 or p = 1.0) the loading degenerates to constant amplitude. At p = 0 the four subsidiary cycles disappear, so that the life under the complex load cycle merely becomes N_c, the constant amplitude life under the peak stress range. At p = 1.0 all the cycles (one main and four subsidiary) have the same magnitude, so that the life in 'blocks' (where a block is defined as consisting of the main constant amplitude cycle and all its associated subsid- iary cycles) becomes $N_c/5$. It will be seen from Fig. 3 that there is an excellent linear relationship between p and Ln (N_B), where N_B is the life measured in 'blocks', joining these two end points. The relationship between p and N_B is therefore

$$N_B = N_c (1 + v)^{-p}$$

where v is the number of subsidiary cycles per block (4 in Fig. 3).

For comparison, the lives required to give $\Sigma\frac{n}{N}$ = 1.0 are also indicated. As noted above, it is clear that the actual values of $\Sigma\frac{n}{N}$ were consistently less than 1.0, except at the two limits (p = 0 and p = 1.0).

The same general form of behaviour was found to occur with each of the loading blocks shown in Fig. 2. It was also found with as-welded specimens subjected to an alternating, rather than pulsating tension, main cycle and with stress relieved specimens under a pulsating tension cycle. Anomalies were found, however, with stress relieved specimens subjected to an alternating main cycle, particularly when the subsidiary cycles were at a different mean stress so that they were either fully tensile or fully compressive. This problem of the influence of mean stress in stress relieved specimens remains to be fully resolved.

If one assumes (even if there is no obvious reason for it) that the behaviour indicated in Fig. 3 will also occur when there are subsidiary cycles of several different magnitudes associated with each main cycle, instead of only one, it is easy to deduce that the expected life (in blocks) can be written as

$$N_B = N_c \ e^{-Area}$$

Stress	Exceedences	Area
1.0	1 +	0
p_1	$N_{E_1} = 1 + V_1$	$p_1\ Ln\ (N_{E_1})$
p_2	$N_{E_2} = 1 + V_1 + V_2$	$p_2\ \{Ln\ (N_{E_2}) - Ln\ (N_{E_1})\}$

Total area $= (p_1 - p_2)\ Ln(N_{E_1}) + p_2\ Ln(N_{E_2})$

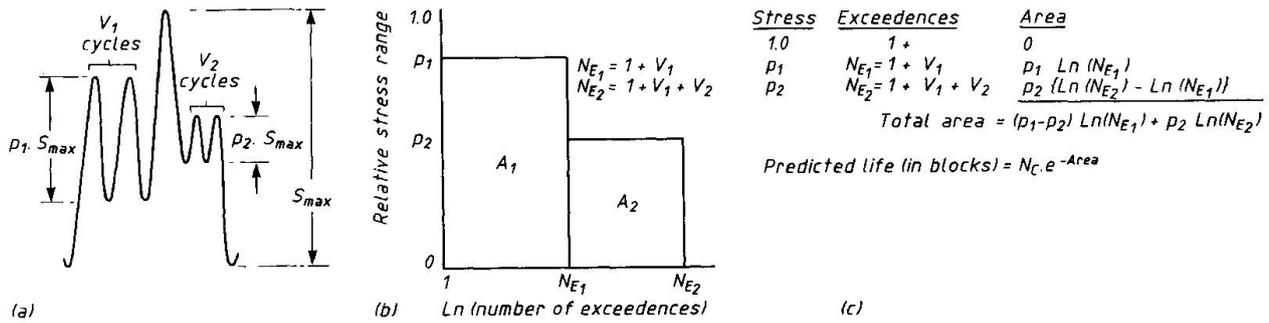Predicted life (in blocks) $= N_C . e^{-Area}$

Fig.4 Example of life calculation using the area rule
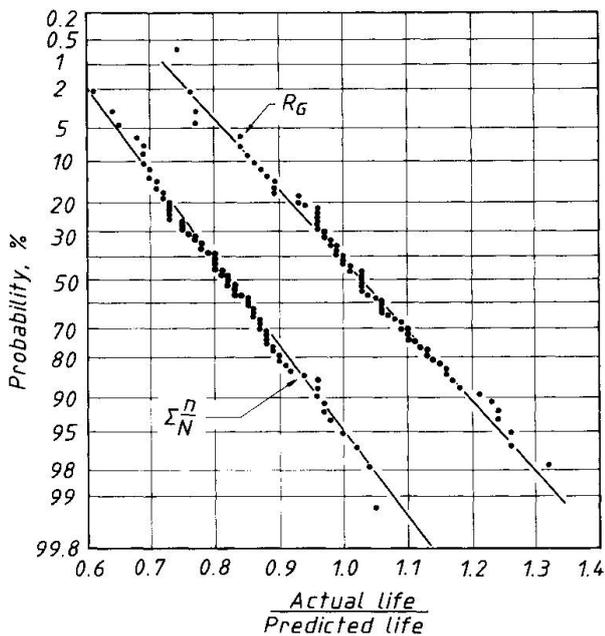

Fig.5 Comparison of Miner's rule and
     area rule for short blocks

where 'Area' is the area under the p v. Ln N_E exceedence diagram for the loading spectrum, N_{E_i} being the number of exceedences of stress p_i per block. A simple example is shown in Fig. 4. Like Miner's rule, the 'area rule' at least has the merit of simplicity. The problem is, 'Is it any better?' In order to make the comparison it is convenient to express experimental results in terms of the ratio R_G (= actual life/life predicted by the area rule). This is directly comparable to the value $\Sigma\frac{n}{N}$ for Miner's rule.

A summary of all the results obtained for very simple loading of the type shown in Fig. 2, but ignoring the results for stress relieved specimens under alternating loading (where special considerations apply) is shown in Fig. 5. Clearly for those types of loading the area rule is superior to Miner's rule.

The next step was therefore to compare the two under more complex load spectra and the initial tests [5] involved Rayleigh distributions of stress ranges of various block lengths (and hence various clipping ratios). In all cases the individual cycles forming a block were applied in random order at R = 0 and the block was then repeated, in the same order, until failure occurred.

The results, in terms of $\Sigma\frac{n}{N}$, are shown in Fig. 6(a). They show two interesting features:

1.   a clear tendency for $\Sigma\frac{n}{N}$ to increase with increasing block length

2.   an equally clear tendency for $\Sigma\frac{n}{N}$ to decrease as the stress magnitude is decreased.

In other words, at least for this particular type of spectrum, the trends suggest that Miner's rule would become unsafe at short block lengths, with the critical block length increasing as the applied stresses decrease.

In contrast, the results expressed in terms of the area rule were all safe (Fig. 6(b)), although their trend suggested that it might well become unsafe at very long block lengths (approx. 10^6 cycles). On the other hand, the great accuracy of the prediction for the very simple type of loading obviously did not carry through to these particular tests, since R_G obviously rose to a peak at a block
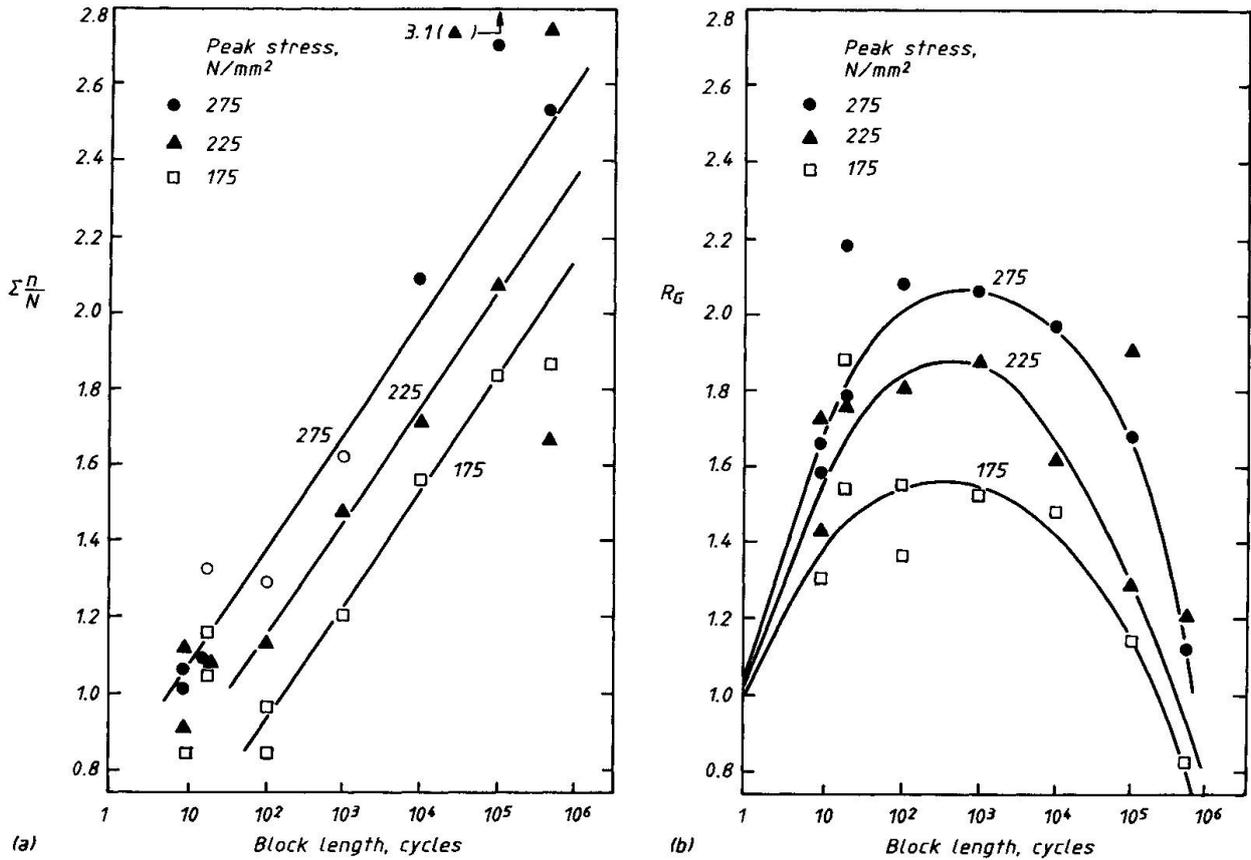
Fig.6 Influence of block length on (a) $\Sigma\frac{n}{N}$ and (b) R_G for Rayleigh spectra

length of about 10^3 cycles before reducing again; equally, like the value of $\Sigma\frac{n}{N}$, R_G was obviously also a function of the stress magnitude.

In passing, it is worth noting that these results show, quite conclusively, that there is little benefit to be gained by working in terms of 'equivalent stress' (cube root mean cube stress range) or any variety of rms stress. As can be seen from Fig. 7 the use of these parameters does not normalise the results to a single curve. Not only do results at different stress ranges with the same spectrum plot on different curves, but so do the results for different spectra (in this case Rayleigh and Laplace).

Endurance, cycles
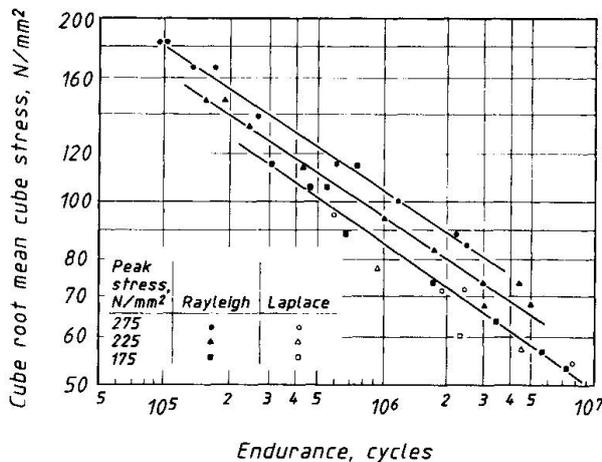
Fig.7 Results for Rayleigh
and Laplace spectra

As stated previously, one interpretation of the results in Fig. 6 is that $\Sigma\frac{n}{N}$ tends to increase as block length increases, but an equally good interpretation, since clipping ratio is related to block length, is that $\Sigma\frac{n}{N}$ tends to increase as clipping ratio increases. Since they are related it is impossible, for any particular shape of spectrum, to determine which is the more relevant variable. However, by varying spectrum shape as well, it was possible to carry out tests with the same block lengths but different clipping ratios and also with the same clipping ratios but different block lengths. The spectra were based upon the 2 parameter Weibull

distribution and the results again showed that both $\Sigma\frac{n}{N}$ and R_G tended to decrease as the stress level decreased; at 275 N/mm^2 the values were typically 19% higher than at 175 N/mm^2. It was therefore possible to increase the database by applying that correction and assuming that all specimens were tested at 275 N/mm^2.

Analysis of the results after applying that correction showed that the value of $\Sigma\frac{n}{N}$ was almost completely insensitive to clipping ratio but, as with the Rayleigh spectra (Fig. 6(a)) there was again a fairly general tendency for $\Sigma\frac{n}{N}$ to increase with increasing block length, although there were some 'outlying' results. Similarly, the influence of block length on the value of R_G appeared to be very like that shown in Fig. 6(b).

Since these results appear to show that R_G gives safe predictions of life at short block lengths but that they become unsafe at long block lengths, all the available test data from the literature were re-analysed in order to derive the values of R_G at failure. The results are summarised in Fig. 8, but it does not include those for very short block lengths, which were summarised in Fig. 5. For relatively short block lengths (up to 10^5 cycles) the results were nearly all 'safe', even with N_c derived from the mean S-N curves. If the mean $-$ 2 SD design curves had been used, only 2 results would have been 'unsafe'. However, it is clear that, for long block lengths ($\geq 2 \times 10^5$ cycles), R_G certainly does tend to become unsafe.
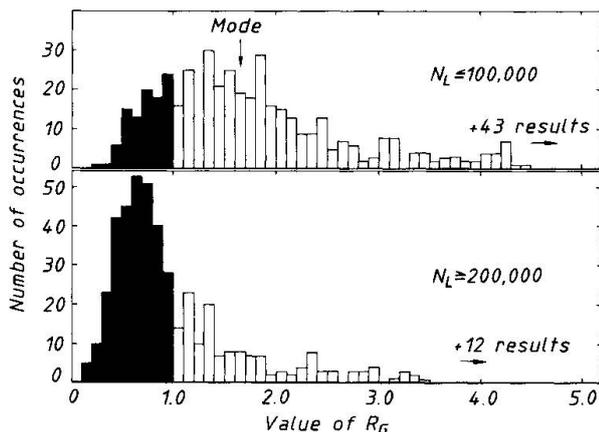

Fig.8 Summary of values of R_G

Up to this point all the results considered, except a few of the tests with very simple stress cycles (Fig. 2), involved all the cycles being applied at R = 0. The next stage therefore involved some exploratory tests to study the influence of stress ratio and mean stress. They were based upon 2 stress spectra, each with a block length of 128 cycles. The particular variants which were employed were:

a) All cycles at R = 0, random order

b) All cycles at R = -1, same order

c) All cycles with the same S_{max}, again in the same order (cf stalactites)

d) With the peak cycle at R = 0 or R = -1 but with the stress ratios of the other cycles varied within the overall range of the peak cycle (i.e. wide band loading). Again the order of the cycles was the same as before.

e) With the cycles arranged in decreasing-increasing order, as in a typical block programme test. These tests involved all cycles being at the same stress ratio (R = 0 and R = -1).

Apart from (e), all variants had the same stress ranges applied in the same order so that, in terms of stress range, their rainflow (or reservoir) counts were identical.

The average values of $\Sigma\frac{n}{N}$ which were obtained are summarised in Table 1. It is obvious that there was a tendency for $\Sigma\frac{n}{N}$ to be lower under alternating than under pulsating tension loading, although the difference was small under wide band loading. Surprisingly, extremely few other tests seem to have been carried out at R = - 1 except under programmed block loading. A comparison of those results with similar ones obtained at R = 0 is shown in Fig. 9. In that case also, there was a reduction in $\Sigma\frac{n}{N}$ at R = - 1, typically of about 28%. While there is obviously a need for more information this evidence does suggest that

Type of loading	Peak stress at	
	R = 0	R = -1
All cycles at same stress ratio, in random order	1.32	0.75
'Stalactitic' spectrum	0.55	
Decreasing-increasing block programme	1.59	0.88
Wide band (variable R)	0.80	0.75

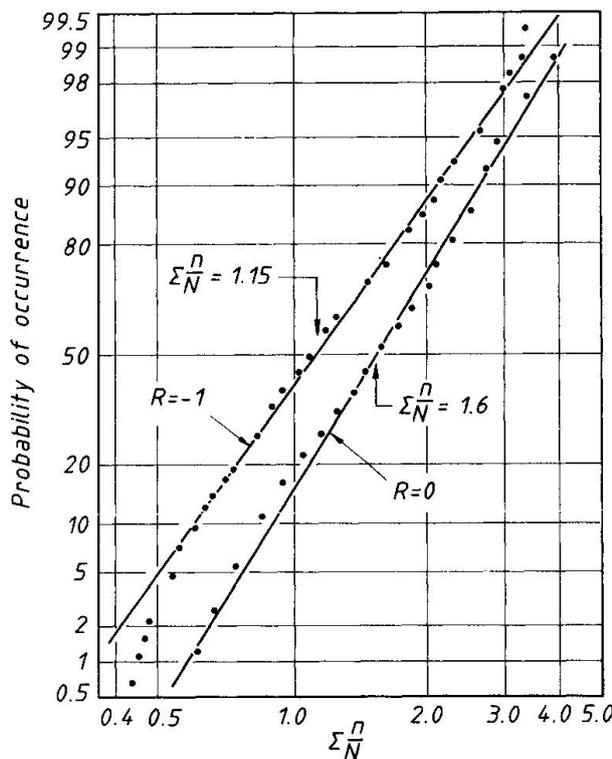Table 1 Values of $\Sigma\frac{n}{N}$ using different
types of loading

Fig.9 Effect of R on values of $\Sigma\frac{n}{N}$
for block programme tests

lower values of $\Sigma\frac{n}{N}$ are to be
expected under alternating load-
ing.

Similarly the tests in which all
the cycles had the same maximum
stress (what one might call a
stalactitic spectrum) also gave a
much lower value of $\Sigma\frac{n}{N}$, with a
typical value of $\Sigma\frac{n}{N} = 0.55$. That
is very similar to the value
obtained by Maddox in similar tests
using the BS 5400 Axle loading
spectrum. These were, incident-
ally, the results which were
omitted omitted from Fig. 1. The
original idea behind testing with
this type of spectrum was that it
would be an easy way to simulate
the presence of high tensile
residual stresses, which would be
expected to be present in a large
structure, in a small specimen. If
correct, the results are obviously
a little worrying, but it remains
to be proved whether or not this
method of simulation is too severe.

Turning now to the effect of wide
band loading, the results were
analysed using the S-N curves cor-
responding to the stress ratio of
the peak stress ange, regardless of
the fact that most of the smaller
cycles were at different stress
ratios. On this basis the values
of $\Sigma\frac{n}{N}$ were very similar for the two
stress ratios and ranged from
approximately 0.5 - 1.0 with a mean
value of about 0.76.

In the context of whether or not
one should use Miner's rule to
design structures subjected to such
loading, this result is also a
little worrying, particularly bear-
ing in mind the numbers of speci-
mens for which the predicted lives
were safe or unsafe (see Table 2).
On the other hand, the Area rule
did appear to give either safe or acceptable predictions with these particular
spectra. It must be remembered, however, that all these tests were carried out
using spectra with relatively short block lengths (128 cycles); it has yet to be
proved whether or not the results are block length dependent under wide band
loading.

Finally, the opportunity was taken to obtain comparative results for the same
spectra but with the individual cycles arranged in decreasing-increasing order,
so as to simulate a typical block programme test. In this way it was hoped to
obtain some evidence as to the likely accuracy of other block programme tests,
since such results make up a very large proportion of the variable amplitude

Type of loading	No. of tests	Miner's rule		Area rule	
		>1.0	≥1.0	<1.0	≥1.0
Peak stress at R = 0					
All cycles at R = 0	4	–	4	–	4
All cycles with peak stress = S_{max}	4	4	–	1	3
Ordered block loading	7	–	7	–	7
Wide band loading	24	23	1	–	24
Peak stress at R = -1					
All cycles at R = -1	4	4	–	–	4
Ordered block loading	5	4	1	–	5
Wide band loading	29	28	1	10	19

Table 2 Summary of numbers of safe and unsafe predictions using Miner's rule and the 'area' rule

database and, as far as is known, no other directly comparable tests have been reported previously.

As can be seen from the summary of the results set out above, there was a substantial difference between the 'block programme' results and the 'random order' results at both stress ratios; typically the value of $\Sigma\frac{n}{N}$ obtained under block programme loading was 20% higher at both stress ratios. Clearly this must cast some doubt on the validity of all the earlier block programme results and it is obvious that further check tests are required for other types of spectra.

3. SUMMARY OF THE CURRENT POSITION AND FUTURE WORK REQUIREMENTS

As was shown at the beginning of this review, the available experimental evidence indicates that Miner's rule, based on the mean − 2 S.D. design S–N curves, should be a satisfactory design method in most situations. Nevertheless, there are clearly some where it may be unsafe.

The most obvious of these is when the loading involves short block lengths − in other words when the peak stress in the spectrum occurs fairly frequently. A typical example might be an overhead travelling crane working on a production process. Similarly, certain types of earth−moving plant, where the machine essentially goes through a continuous series of digging and unloading cycles, might also qualify. There are almost certainly many other examples. The evidence certainly seems to suggest that the 'area rule' would be an advance on Miner's rule for dealing with this particular type of loading.

The second major problem area seems to be the tendency for $\Sigma\frac{n}{N}$ to decrease as the applied stresses decrease. It is a trend which seems to be very evident under tensile loading when the individual stress ranges in the spectrum are applied in random order and when the peak stresses are fairly high. Much work is, however, still needed to confirm the extent to which the trend continues to lower stresses and also whether it also applies at other stress ratios and mean stresses.

If it is a general problem it would be worrying for two reasons. In the first place, almost the whole database of variable amplitude test results, which justify the continued use of Miner's rule, would be suspect. After all, nearly all the tests have, quite deliberately, been carried out at relatively high stresses in order to give shortish lives and hence reduce testing costs.

Secondly, many structures have been designed at much lower stresses, which implies that their lives might become much shorter than expected. Although it is easy to understand why tests have largely been restricted to high stresses and short lives, there is obviously a need to obtain data for more realistic stresses and longer lives.

Associated with this problem of decreasing $\Sigma\frac{n}{N}$ as stresses decrease is, of course, the question of what constitutes a 'short block length' at low applied stresses. Clearly, one would expect the critical block length to increase, but by how much will certainly need to be established.

In the light of the evidence pointing to a marked reduction in the value of $\Sigma\frac{n}{N}$ at R = -1 as compared to R = 0, and also under 'stalactitic' loading with a constant maximum tensile stress, there is also a need to investigate the influence of mean stress. In particular, it needs to be established whether stalactitic loading is a realistic simulation of the high tensile residual stresses which may occur in actual structures, and also whether the use of S-N curves related to stress range alone (i.e. ignoring mean stress) is a sensible basis for design under variable amplitude (as opposed to constant amplitude) loading.

The available evidence also suggests that there are likely to be problems under wide band loading, but it must be remembered that that evidence was obtained using short block lengths (128 cycles). It is at least possible that the problems will disappear with longer block lengths, but that is an area which also remains to be investigated.

REFERENCES

1. MINER M.A., Cumulative Damage in Fatigue. J.Appl.Mech., Vol. 12, No. 3, Sept. 1945, pp 159-164.

2. MADDOX S.J., A Fracture Mechanics Approach to Service Load Fatigue in Welded Structures. Weld.Res.Int., Vol. 4, No. 2, 1974, pp 1-30.

3. HAIBACH E., The Fatigue Strength of Welded Joints examined by Local Strain Measurement. LBF Report FB77, 1968.

4. CURNEY T.R., Fatigue Tests on Fillet Welded Joints to assess the Reliability of Miner's Cumulative Damage Rule. Proc.Roy.Soc., 1983, A386, pp 393-408.

5. GURNEY T.R., Some Variable Amplitude Fatigue Tests on Fillet Welded Joints. Conf. 'Fatigue of Welded Constructions', Brighton, April 1987.

Numerical Simulation of Fatigue Crack Growth

Simulation numérique de la propagation de fissures de fatigue

Numerische Simulation des Ermüdungsrisswachstums

Carlo A. CASTIGLIONI
Assist. Professor
Politecnico di Milano
Milan, Italy

Carlo A. Castiglioni, born 1956, is currently an Assistant Professor at the Structural Engineering Department, at Politecnico di Milano. After receiving his Laurea in Civil Engineering from Politecnico di Milano in 1980, he was part of the Visiting Faculty at Lehigh University, Bethlehem, PA, USA, in 1984. He is the Italian representative in ECCS Committee 6, «Fatigue» and his main research fields are high and low cycle fatigue of steel structures.

SUMMARY

This paper compares fatigue test data on full-scale structural-steel details under both constant and variable amplitude loading with results obtained through numerical simulation. Objectives include modelling fatigue crack growth in structural details commonly used in steel constructions, such as coverplates and web attachments. Random variability of parameters governing the fatigue crack propagation process is accommodated.

RÉSUMÉ

Cet article compare les résultats d'essais de fatigue sur des détails de structures en acier de dimension réelle sollicités sous charge d'amplitude constante et variable, avec les résultats obtenus à l'aide d'une simulation numérique. L'un des objectifs consiste en la modélisation de la propagation de fissures de fatigue dans des détails couramment utilisés en construction métallique, tels que des semelles de renfort et des liaisons à l'âme. La variation aléatoire des paramètres déterminants pour le comportement des fissures de fatigue est également prise en compte.

ZUSAMMENFASSUNG

Der vorliegende Beitrag vergleicht Resultate aus Ermüdungsversuchen an Bauteilen, die sowohl unter konstanter wie auch variabler Spannungsamplitude durchgeführt wurden, mit Resultaten aus entsprechenden numerischen Simulationen. Eines der angestrebten Ziele ist es, das Wachstum von Ermüdungsrissen, ausgehend von gebräuchlichen Stahlbau-Konstruktionsdetails, wie beispielsweise Lamellen oder auf Stege aufgeschweisste Laschen, modellieren zu können. Die Streuung der für den Rissverlauf massgebenden Parameter wird berücksichtigt.

1. INTRODUCTION

Although in reality fatigue cracking is generally caused by random variable
amplitude loading, to date there are very few available results of long life
($N>10^7$ cycles), variable amplitude loading fatigue tests carried out on full
scale structural elements [1]. This is due to the fact that full scale, random
loading fatigue testing, in the long endurance range, requires long testing
periods, with very high costs. While experimental research is absolutely
necessary and fundamental, the time and money needed for this type of approach
induces to take into consideration the possibility of studying numerical
procedures that, calibrated on few test results, may be able to supply useful
indications and improve our understanding of the problem under investigation.
Though a series of numerical models of fatigue crack growth are already
available in the literature [2-10], they deal with cases of ideal growth and
are not aimed at the study of details typically adopted in steel
constructions. Furthermore, for one way or another, none of the models to the
author's knowledge, can be regarded as complitely satisfactory for the
simulation of fatigue crack growth in structural steel details. In fact, the
existing numerical models can be subdivided into three main groups:
1) deterministic models, like [2], that allow the simulation of the detail
   behavior during all phases of crack growth (fig. 1.1);
2) probabilistic approaches, capable of interpreting the low frequency random
   aspects of crack growth, by assuming the coefficients in the crack
   propagation law as random variables (fig. 1.2);
3) probabilistic approaches, capable of interpreting, during the intermediate,
   linear, phase of crack growth even the high frequency aleatory components,
   by means of the superposition of the Paris's Law with a random noise (fig.
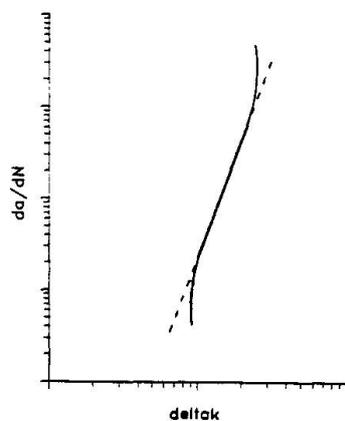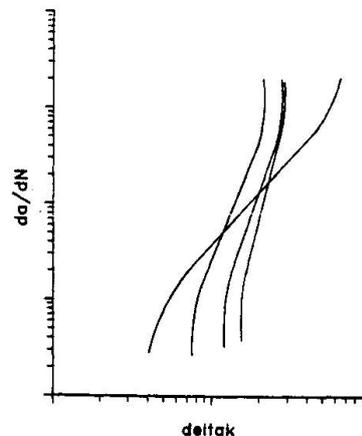   1.3).

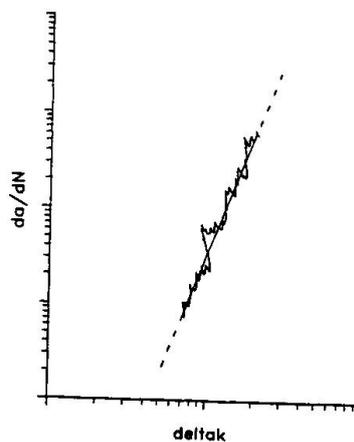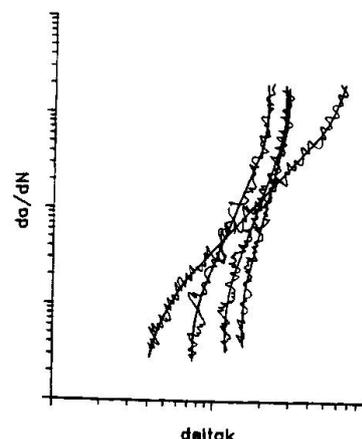Fig. 1.1

Fig. 1.2

Fig. 1.3

Fig. 1.4

Recently, Castiglioni and Rossi [11] proposed a numerical model that encompasses the characteristics of all the three types discussed above (fig. 1.4), i.e. capable of simulating both types of random non-homogeneity (at high and low frequency), even in the two extreme phases of crack growth, i.e. in proximity of the threshold value ΔK_{th} and of the critical one ΔK_c of the stress intensity factor range.

In fact, a propagation law is assumed of the type:

$$da/dN = f(\Delta K) \; Z(a) \tag{1}$$

in which $Z(a)$ is a random function, as proposed in [9], and $f(\Delta K)$ is the deterministic function proposed by Newman [12]:

$$f(\Delta K) = C \; (1 - R)^m \; \Delta K^n \; (\Delta K - \Delta K_{th})^p \; [(1 - R)K_c - \Delta K]^{-q} \tag{2}$$

where C, m, n, p and q are material dependent parameters, considered to be random variables. It is immediately recognized that (2) as a whole includes the most commonly used propagation laws, as Paris's (m=p=q=0), Forman's (m=p=q=1) and Walker's (p=q=0, m=n[m_w-1]).

The model presented in [11] takes into account:
1) various crack configurations and loading conditions (fig. 2)
2) retardation effects due to overloading according to Willenborg's model [13]
3) crack closure according to Newman's model [14]
4) stress concentrations due to geometric effects, and relative stress intensity factor's correction factors
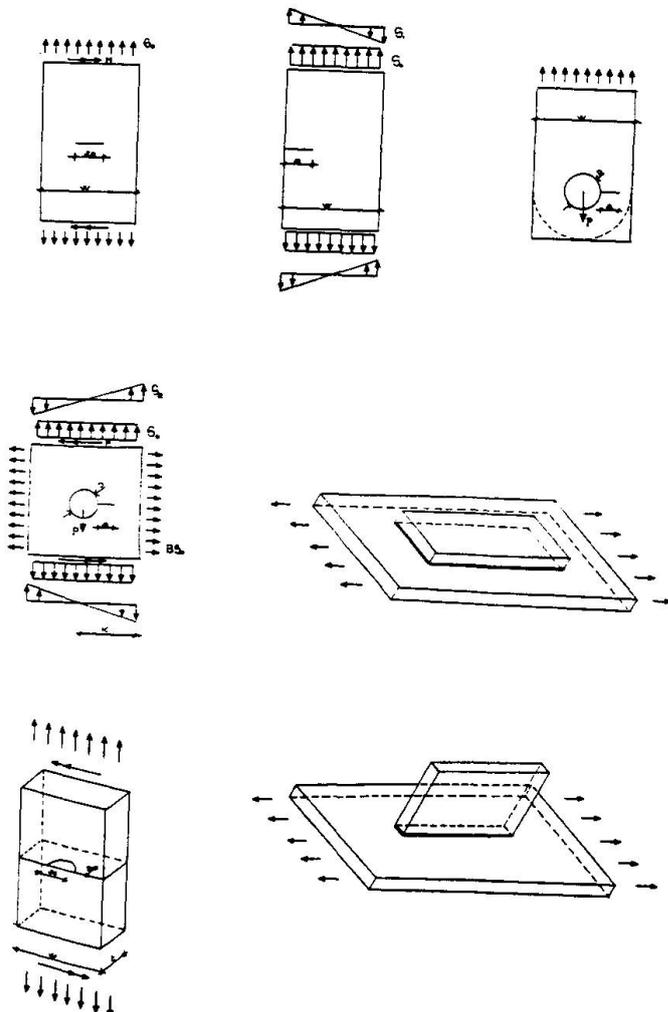5) stress corrosion

Fig. 2

In this paper, some results are presented obtained by means of model [11]. The behavior of typical structural steel details is simulated and the numerical results are compared with those of available experimental tests. In the case of fatigue under constant amplitude loading cycles, the results reported in the literature [15-17], relating to the weld toes at the ends of web attachments and of coverplates on beam flanges, are taken into consideration. Finally the influence of the loading history on the fatigue life of some structural details is investigated. To begin with, in order to determine the correspondence of the model with the physical reality, the case is considered of a plate with a through crack, for which the test results are widely presented in the literature. Attention is then focused on longitudinal web attachments and, in order to make a comparison, geometries similar to those adopted in the tests presented in [18] are considered.

2. ANALYSIS OF THE RESULTS

In order to correctly simulate fatigue tests on typical structural details, the model was previously calibrated [11] on the basis of available experimental results. In [11], at first the effect of the single parameters governing the model is investigated, with reference to the simple case of a plate with a through crack. It is concluded that the variability of the parameters of the propagation law (functions of the material), during crack growth, does not substantially influence the fatigue life of the structural detail. On the contrary, the superposition to the propagation law of a high frequency noise $Z(a)$, defined by a stationary stochastic process with a log-normal statistics has an influence on the fatigue life that is comparable with that of the initial defect size.

In this paper, the simulation of some experimental tests on full scale beams is presented. Furthermore, the influence of the loading history is investigated, with reference to the case of a plate with a through crack.

2.1 Constant Amplitude Loading

The test results reported in [15-17], concerning coverplated beams and web attachments are taken into consideration.
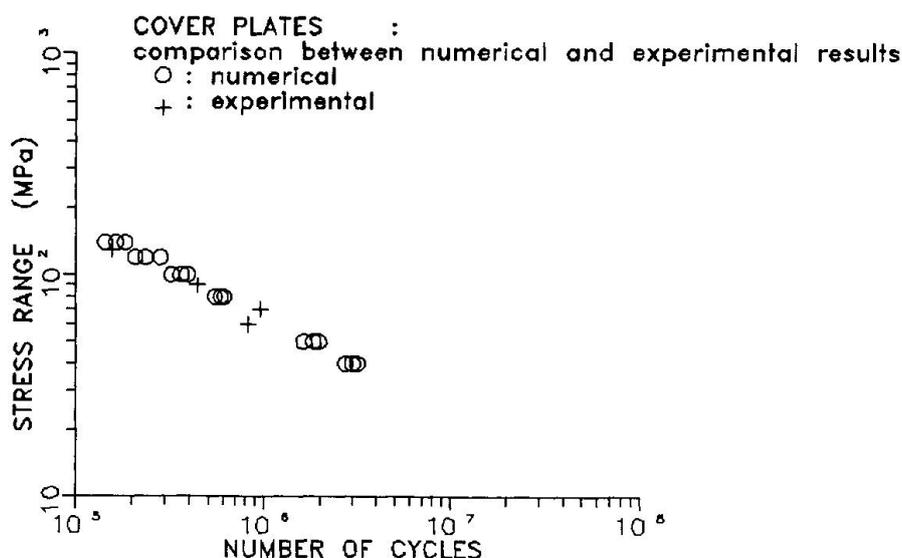

Fig. 3

Various numerical simulations were carried out at the same stress range level, considering different initial crack depths chosen from a sample having a normal distribution, 0.1 mm mean value and 40% standard deviation. The crack shape correction factor was computed, as a function of the crack size (a), with reference to the relationships between crack depth (a) and crack width (c) proposed, for both coverplates and web attachments by Fisher [19].

The parameters of the crack propagation law were calibrated on the test data presented in [18] for a plate with a central through crack, while the material parameters were obtained from [16,17].

Fig. 3 shows a comparison between numerical and experimental results in the case of coverplates on beam flanges.

It can be noticed that the numerical results interpret fairly well the trend of the experimental data, at all the stress range levels considered.

Fig. 4 shows the comparison between experimental test data and numerical simulation results in the case of web attachments. Also in this case it can be noticed that the numerical simulation interprets fairly well the trend of the experimental data.

Examining fig. 4 it can be noticed that the scattering in the numerical results is greater for the lower stress ranges than for the higher ones. This is also in agreement with the experimental evidence.

It is important to notice that, from both figs. 3 and 4, independently on the stress range level, it is evident a greater scattering in the experimental
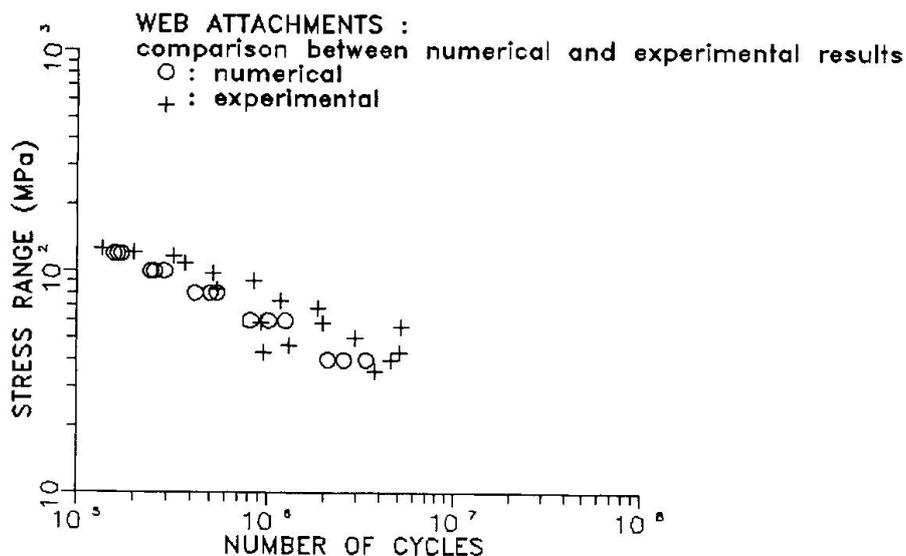
Fig. 4

data than in the numerical ones. This is probably due to two main reasons:
- the actual initial defect size is greater than that assumed in the numerical simulation. This fact might be easily corrected by generating a new sample of initial defects, with a larger mean value and standard deviation;
- the presence of residual stresses due to the welding process influences relevantly the fatigue life of actual welded components, as widely demonstrated and discussed in the literature [19,20]. Of course, the statistics of the residual stress distributions are characterized by large standard deviations from the mean value, depending on such factors as, for example, the plates' thickness and the welding process. In the numerical

model, at the present state, the presence of residual stresses in the joints is complitely disregarded, thus reducing the possible causes of randomness, and the scattering of the results.

From examining both figures 3 and 4, however, it can be concluded that the numerical model is capable of predicting the fatigue life of web attachments and coverplated beams under constant amplitude loading in fairly good agreement with the experimental results.

2.2 Variable Amplitude Loading

2.2.1 Influence of the Loading History

In order to verify the model's capacity to interpret the loading spectrum's influence on fatigue life, a plate similar to the one shown in fig. 5 is first examined.
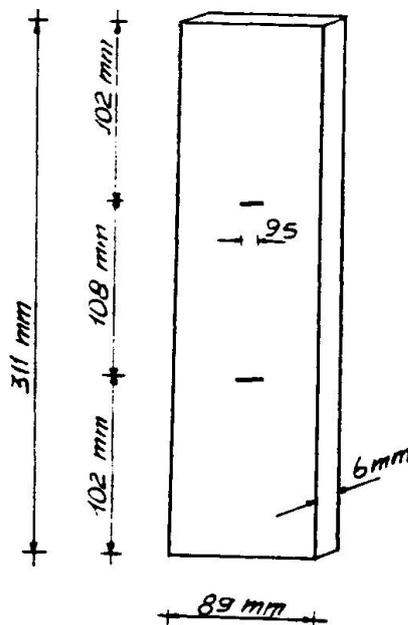
A set of random loading histories, with a Rayleigh type distribution of the variable amplitude loading cycles are generated, with stress ranges S ranging from 5 MPa to 13.5 MPa.

The loading histories differ from one another either in the value of the stress ratio R between the minimum and maximum stress, or in the exceedence rate γ, i.e. the probability that the maximum cycle amplitude (S_{max}) exceeds a specific limit value (S_{lim}). Stress ratios R=0.5 and 0.7, and exceedance rates γ=0.1%, 1% and 5% were considered. Furthermore, for fixed R and γ values, three loading histories are randomly generated, each one different from the other only for the sequence of the stress ranges. Each loading history consists of a block of 5,000 cycles, repeatedly imposed on the simulated specimen until collapse situation is reached; in any case the simulation was interrupted after a maximum of 50,000 repetitions (equivalent to 250×10^6 cycles).

Fig. 5

The results obtained are presented in fig. 6, where the simulated fatigue lives (N) are plotted against the root mean cube (equivalent) stress range,

$$S_{eq} = (\Sigma_i \, \alpha_i \, S_i^3)^{1/3} \qquad\qquad (3)$$

By examining fig. 6 it can be noticed how the model can interpret the effect of the stress ratio R, on the fatigue life. In fact, for each exceedance rate level, the numerical model predicted shorter endurances for those specimens subjected to stress histories associated with the higher R ratios (R=0.7).

The effect of the exceedance rate on fatigue life is also evident, in fact, for a fixed R ratio value, decreasing γ results in longer endurances.

By examining fig. 6 it can also be noticed that fatigue life is strongly influenced not only by the stress ratio R and the exceedance rate γ, but also by the loading sequence. In fact, for R=0.5 and γ=0.1%, certain cases did not reach critical conditions after 250×10^6 cycles, and are plotted in fig. 6 as run-outs.

EFFECTS OF LOADING SEQUENCE
R=0.5 :   △ γ =0.05   —   R=0.7 :   × γ =0.05
             o γ =0.01   —   + γ =0.01
             ☆ γ =0.001   —   * γ =0.001
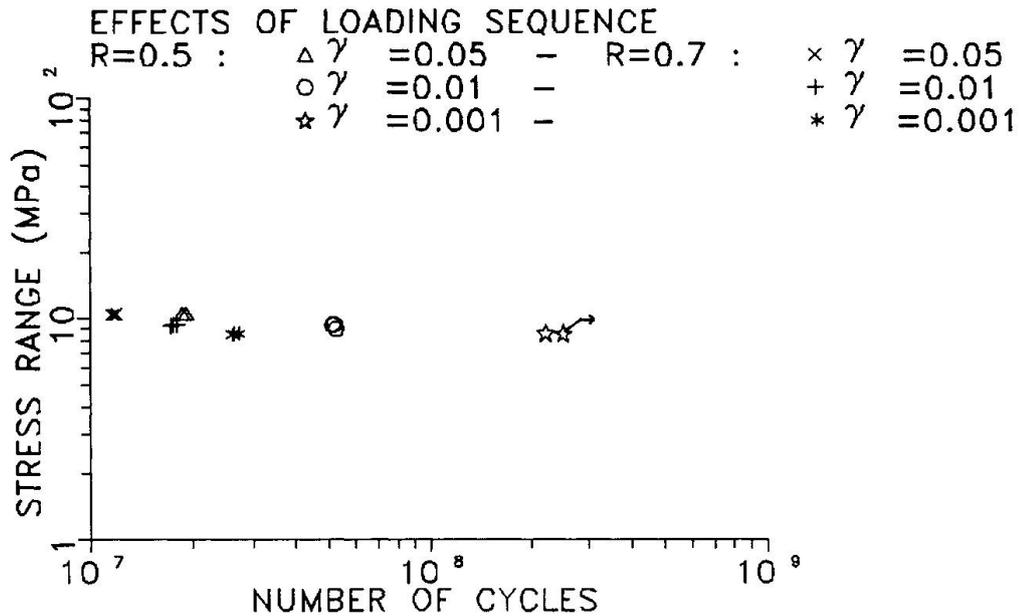

Fig. 6

It can be concluded that the numerical results are in good agreement with the physical reality, though it is not possible to make comparisons with the experimental results reported in [9], because these were obtained by varying in each case the stress range, both in order to compensate the effects due to the increase in crack size and to get as close as possible to the threshold value.

2.2.2 Simulation of Web Attachments

Finally, an attempt is made to simulate some of the experimental tests on web attachments under variable amplitude loading by Fisher, Mertz and Zhong, reported in [18].

The various numerical simulations were carried out considering different initial crack depths chosen from a sample having a normal distribution, 0.1 mm mean value and 40% standard deviation.

Loading histories are generated, similar to those adopted in the experimental tests [18], and consisting of a block of 5,000 cycles, repeatedly imposed on the joint. This loading history has a probability $\gamma=0.1\%$ that the maximum stress range exceeds the value $S_{lim}=$ 31 MPa, assumed by the AASHTO Specifications [21] as the constant amplitude fatigue limit for this structural detail.

The comparison between the experimental data and the numerical simulation results is presented in fig. 7, where the number of cycles (N) is plotted against the root mean cube (Miner's) equivalent stress range (S_{eq}).

A reasonable agreement between numerical and experimental results can be noticed by examining fig. 7, confirming the remarkable versatility and acceptable reliability of the numerical model [11].
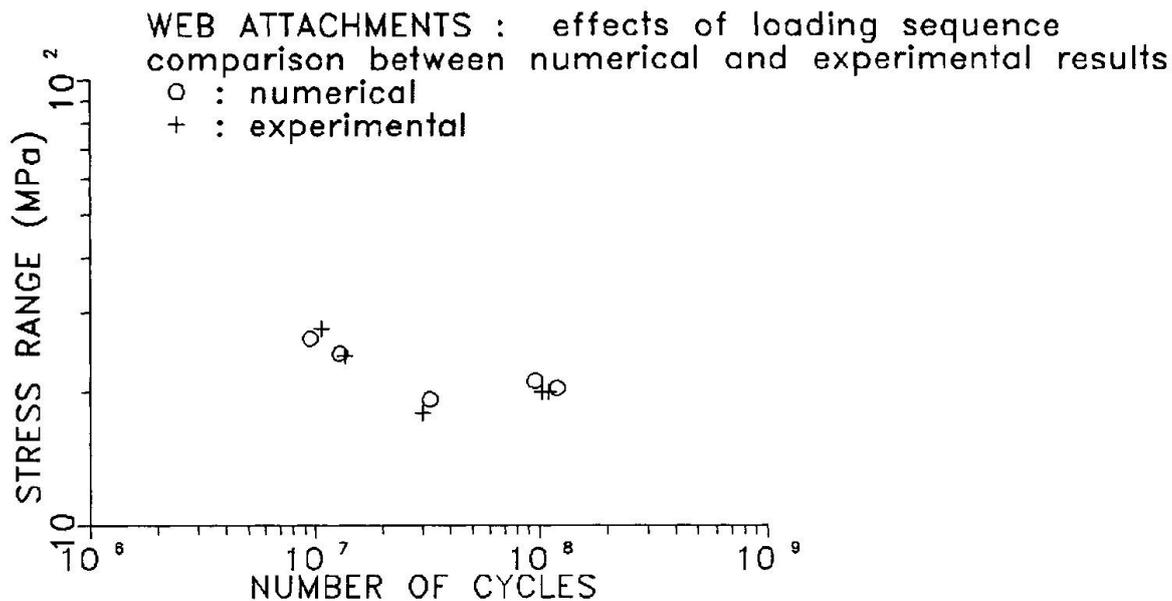
Fig. 7

3. CONCLUSIONS

Although the model presented in [11], in its present state, can be furtherly improved by implementing the possibility of considering for example the presence of residual stresses and/or other geometries and structutal details, it nevertheless seems to be a valid starting point for a reliable numerical simulation of fatigue crack growth in structural steel details (both welded and unwelded).

The good agreement between numerical and experimental results has been shown in this paper, by comparing experimental test data with numerical results.

Once the reliability of the model has been checked on the basis of available experimental test data, attention can be focused on its possible future applications.

Two main field can be immediately identified, one regarding its use for increasing the available data base in the long life region ($N>50\times10^6$ cycles), the other aimed to the prediction of the fatigue life of a given component subjected to a known loading history.

In the first case, the model can be calibrated on a few test data either available or obtainable submitting the structural detail to constant amplitude loading, even at relatively high stress range levels. Once the model is calibrated, estimates of the fatigue life can be obtained by projection into the long endurance range. From this estimates trends can be identified rather quickly, avoiding the lengthy and expensive experimental long life fatigue tests. These will be in fact necessary only in a limited number, in order to double-check the numerical estimates obtained.

Adoption of the model for estimating the remaining fatigue life of a given component might be more difficult because it requires, in addition to the test data on which the model must be calibrated, also precise informations about the loading history experienced by the component during the service life, and an estimate of the future loading conditions. This last one is however a problem which is common to whatever procedure for estimating the remaining fatigue life of a structural detail, and does not represent an handicap of the presented numerical model.

4. AKNOWLEDGEMENTS

5. REFERENCES

[1] Keating, P.B., Fisher, J.W. "Evaluation of fatigue tests and design criteria on welded details", NCHRP rept. 286, 1986.

[2] ESACRACK, User's Manual ESA PSS-03-209, European Space Agency, May, 1989.

[3] Arone, R., "Influence of random overloads on fatigue crack lifetime and reliability", Engineering Fracture Mechanics, Vol. 30, n.3, 1989.

[4] Langley, R.S., "Stochastic models of fatigue crack growth", Engineering Fracture Mechanics, Vol. 32, n.1, 1989.

[5] Ihara, C., Misawa, T., "A stochastic model for fatigue crack propagation with random propagation resistance", Engineering Fracture Mechanics, Vol. 31, n.1, 1988.

[6] Salivar, G.C., Yang, J.N., Schwartz, B.J., "A statistical model for the prediction of fatigue crack growth under a block type spectrum loading", Engineering Fracture Mechanics, Vol. 31, n.3, 1988.

[7] Alawi, H., "A probabilistic model for fatigue crack growth under random loading", Engineering Fracture Mechanics, Vol. 23, n.3, 1986.

[8] Ortiz, K., Kiremidjian, A.S., "Time series analysis of fatigue crack growth rate data", Engineering Fracture Mechanics, Vol. 24, n.4, 1986.

[9] Ortiz, K., Kiremidjian, A.S., "Stochastic modelling of fatigue crack growth", Engineering Fracture Mechanics, Vol. 29, n.3, 1988.

[10] Ortiz, K., "On stochastic modelling of fatigue crack growth", PhD. Thesis, Stanford University, 1985.

[11] Castiglioni, C.A., Rossi, S., "Un modello stocastico per la stima della vita a fatica di dettagli strutturali in acciaio", Technical Report 7/89, Structural Engineering Department, Politecnico di Milano, Italy.

[12] Newman, J.C.Jr., Raju, I.S., "Prediction of fatigue crack growth patterns and lives in three dimensional cracked bodies", VI International Conference on Fracture, New Delhi, India, 1984.

[13] Willenborg, J., Engle, R.M., Wood, H.A., "A crack growth retardation model using an effective stress concept", AFFDL-TM-71-1-FBR, 1971.

[14] Newman, J.C.Jr., "A crack opening stress equation for fatigue crack growth", International Journal of Fracture, Vol. 24, n.3, 1984.

[15] Shilling, C.G., Klippstein, K.H., Barsom, J.M., Blake, G.T., "Fatigue of welded steel bridge members under variable amplitude loading", NCHRP Rept. n.188, 1978.

[16] Fisher, J.W., Hirt, M.A., McNamee, B.M., "Effect of weldments on the fatigue strength of steel beams", NCHRP Rept. n.102, 1970.

[17] Fisher, J.W., Yen, B.T., Klingerman, D.J., McNamee, B.M., "Fatigue strength of steel beams with welded stiffeners and attachments", NCHRP Rept. n.147, 1974.

[18] Fisher, J.W., Mertz, D.R., Zhong, A., "Steel bridge members under variable amplitude long life loading", NCHRP Rept. n.267, 1983.

[19] Fisher, J.W., "Fatigue and Fracture in Steel Bridges. Case Studies", John Wiley & Sons, New York, 1984.

[20] Keating, P.B., "High Cycle Fatigue Behavior of Welded Details Under Variable Amplitude Loading", PhD. Thesis, Lehigh University, 1987.

[21] AASHTO, "Standard Specifications for Highway Bridges", 1983.

Fatigue Crack Growth in Complex Tubular Joints

Propagation de fissures de fatigue dans des joints tubulaires complexes

Ermüdungsrisswachstum in komplexen Verbindungen von Rohrprofilen

Björn SKALLERUD
Research Eng.
SINTEF
Trondheim, Norway

Björn Skallerud, born 1959, received his master of engineering and doctoral degrees at the Norwegian Inst. of Technology. He has been working with problems related to cyclic plasticity and low and high cycle fatigue.

Oddvar I. EIDE
Senior Research Eng.
SINTEF
Trondheim, Norway

Oddvar I. Eide, born 1951, obtained his master of engineering degree at the Norwegian Inst. of Technology. He is performing research in fatigue and fracture of welded structures, in this area he also holds a doctoral degree.

Stig BERGE
Professor
Norw. Inst. of Techn.
Trondheim, Norway

Stig Berge, born 1942, received his master of engineering and doctoral degrees at the Norwegian Inst. of Technology. He is a professor at the Division of Marine Structures, where he teaches and carries out research in the area of fatigue and fracture of offshore structures.

SUMMARY

Fatigue crack growth data from tests of stiffened tubular joints are reported. Fracture mechanics models for part through and through crack growth analysis are presented, and these results are compared with experimental data.

RÉSUMÉ

Des résultats de propagation de fissures de fatigue provenant d'essais sur des joints de tubes raidis sont présentés. D'autre part, des modèles de la mécanique de la rupture pour la propagation de fissures à travers l'épaisseur de la pièce sont également présentés, et ces résultats sont comparés avec les valeurs expérimentales.

ZUSAMMENFASSUNG

Berichtet wird über Resultate aus Versuchen an ausgesteiften Verbindungen röhrenförmiger Profile. Bruchmechanische Modelle zur Analyse des Wachstums durchgehender und nicht-durchgehender Risse werden vorgestellt. Die Resultate dieser Analysen werden mit denjenigen der Versuche verglichen.

1. INTRODUCTION

One common type of stiffened tubular joints is the connection between a brace
and a comparatively much larger chord, like brace column or brace/pontoon
connections of semi-submersible rigs. These connections are based on load
transfer through internal stiffening of the brace into an array of stiffened
deck and bulkhead details in the column or pontoon. Due to the complicated
geometry, it is difficult to calculate the stress flow through structural
details of this type, and in particular to assess realistic stress concentration
factors for the various weld details. Service experience has proved these
joints to be fatigue vulnerable. Similar type of joints may also be used in
deep water jacket structures, in which fatigue damage may become very critical
due to the general problems of detection and repair at great waterdepths.

With the development of fracture mechanics, methods have become available for
calculation of the significance of defects, residual life of cracked structures
etc., which are required in order to establish rational criteria for inspection,
maintenance, and repair procedures. Furthermore, fracture mechanics has proved
to be a useful tool in the analysis of fatigue test data, enabling conclusions
to be drawn on the basis of physical models rather than statistical analysis of
S-N data.

Within a recent research program, fatigue behaviour of simplified but realistic
models of brace/column connections has been studied. The aims of the investiga-
tion were to provide S-N data for this type of structural details. Furthermore,
to investigate crack growth behaviour in this type of joints in order to estab-
lish and verify fracture mechanics models for assessment of residual life and
consequences of cracking if detected. S-N data obtained with the brace/column
models are reported elsewhere [1]. The emphasis in the present paper is on
fracture mechanics modelling and analysis of fatigue crack growth.

2. EXPERIMENTAL INVESTIGATION

2.1 Specimen and loading

The specimens were simplified but realistic models of brace/column connections
with internal stiffening. The main dimensions are shown in Fig. 1. The models
were constructed such that two connections could be tested simultaneously. The
brace dimensions were 711 mm outer diameter and 12.5 mm plate thickness. Due to
the comparatively much larger column dimensions for this type of joints, the
column was modelled by plane plates. Two models were produced. In order to
investigate the effects of external stiffeners on fatigue behaviour of the
present type of joints, one of the models was tested with external gussets at
the brace/column intersection, cf. Fig. 1.

The brace material was spiral welded tube made from structural steel to NVE-36.
The spiral welds were ground flush prior to specimen fabrication. The plate
material was a structural steel to St52-3. The yield strengths were in the
range 360-400 MPa.

The models were produced by manual metal arc welding, using basic electrodes.
All welds were made as fillet welds. Nominal weld throat was 40 per cent of the
plate thickness. The weld details at the end of the internal stiffening in the
brace (Position 3 in Fig. 1) were post weld treated by grinding. All other
welds were in the as-welded condition.

Testing was performed in constant amplitude axial loading using a 2 MN dynamic actuator. The test rig arrangement is shown in Fig. 2. Nominal stress in the braces were measured by strain gauges attached 300 mm from the brace end and spaced 90 degrees around the brace circumference. No global bending of the braces was observed. Measured stresses were within the range 1.0-1.1 of the computed nominal stress in the brace, the stress enhancement being interpreted as effects of local cross sectional imperfections.

During testing, fatigue cracks developed at the brace/column welds (Pos. 1) and at the ends of external gusset (Pos. 2) and internal stiffener (Pos. 3). The welds were periodically checked for crack initiation by spraying white spirit on the surface during testing. Fatigue cracks were then clearly visible by the pumping of liquid in and out of the crack. When cracks were detected, through thickness crack growth was monitored by a high-frequency, alternating current potential drop system. Surface crack lengths were obtained by visual measurements, using white spirit. Fracture surface examinations showed that the use of white spirit also deposited beachmarks at the fracture surfaces. At the end of testing, crack growth data was checked against the surface markings, providing a direct calibration.
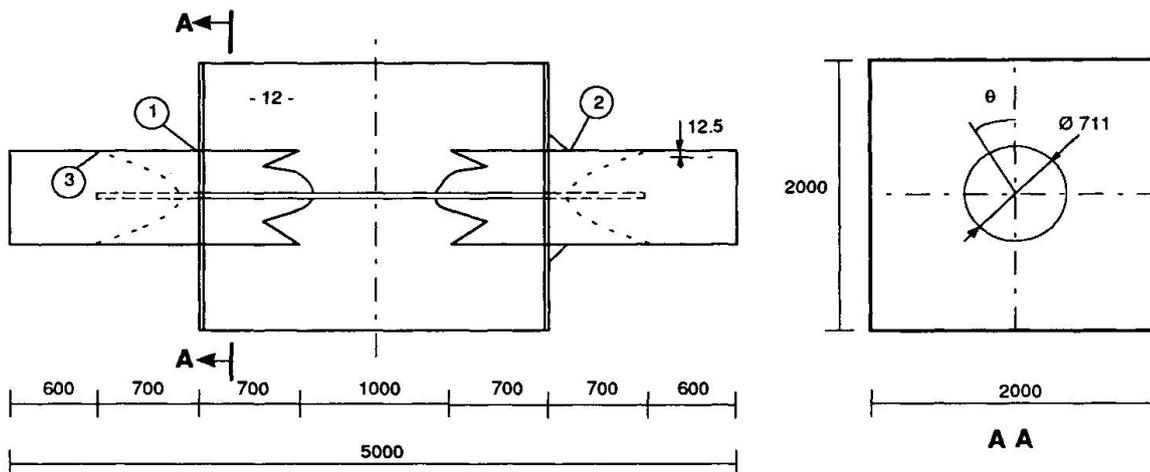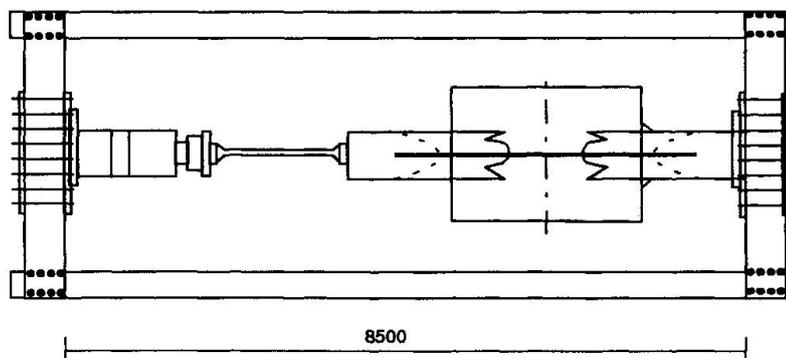
Figure 1   Specimen

Figure 2   Test rig

2.2 Crack initiation and growth

Fracture surface examinations showed that multiple cracks developed along the welds during the first stage of crack growth, i.e. fatigue cracks were initiated at various sites along the weld toe before joining into one single crack (crack coalescence). Typically crack coalescence occurred at a crack depth of 3 mm.

Cracks at the brace column weld (Pos. 1) had a two stage development as shown in Fig. 3. In stage 1, a semi-elliptical surface crack generated from multiple crack initiation was growing in the through thickness direction of the brace wall. Typically 5-7 crack initiation sites were observed in the hot spot region. The surface crack length at the stage of through thickness crack penetration was typically 5-6 times the wall thickness. The through thickness crack was detected by leakage of white spirit.

Once the crack front had penetrated the wall thickness, the crack grew as a three-fronted crack in the brace and in the internal stiffening. Due to significant local bending at the brace/column weld, the growth rate in the brace wall at the external surface significantly exceeded the growth at the internal surface. Crack growth into the internal stiffening was significantly delayed by the root gap of the fillet weld, due to the re-initiation period.

At the end of testing, one of the brace/column weld cracks had reached a surface length of 285 mm. The crack length into the internal stiffening was only 40 mm. The number of cycles applied at this stage exceeded life to through thickness crack penetration by a factor 2.2 approximately. Thus, significant residual life remained after through thickness crack growth at the brace/column weld.

Cracks causing failure at the gusset welds (Pos. 2) went through the same stages of crack growth as observed with the brace/column welds, cf. Fig. 4. In stage 1, however, the occurrence of multiple crack initiation was limited by the length of the gusset end weld. Typically 2-3 cracks developed. Moreover, after crack coalescence, subsequent crack growth in the width direction was delayed by the absence of the notch effect of the weld. For these reasons, the surface crack length at the end of stage 1 was somewhat smaller than observed with the brace/-column welds, being typically 3-4 times the wall thickness.

In stage 2, the transition into a through-thickness crack in the brace occurred within a small number of cycles. For reasons outlined above, crack growth into the internal stiffening was significantly delayed.

At the end of testing, one of the gusset weld cracks had reached a surface crack length of 320 mm. The number of cycles applied at this stage exceeded life to through thickness crack penetration by a factor 1.6 approximately. With reference to similar data obtained with the brace/column welds (Pos. 1) this is a significant reduction in residual life. In average, the growth of through thickness cracks at Pos. 2 was twice as large as the growth observed at Pos. 1. The total effect of the gusset was to increase the life to through thickness penetration, and to reduce residual fatigue life in stage 2 almost correspondingly.
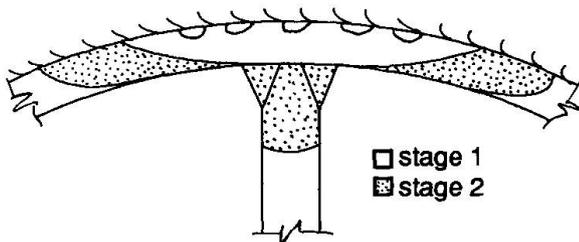
Figure 3   Stages of crack growth at
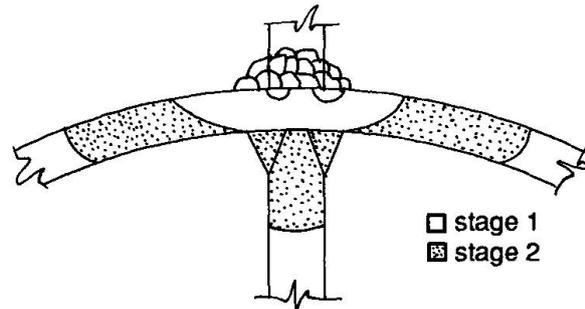brace/column welds

Figure 4   Stages of crack growth at
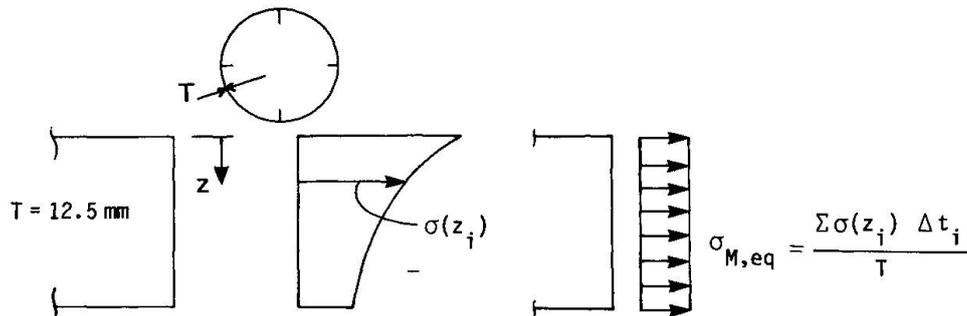external stiffener details

$T = 12.5\,mm$

$\sigma(z_i)$

$$\sigma_{M,eq} = \frac{\Sigma\sigma(z_i)\,\Delta t_i}{T}$$

Figure 5

3. FRACTURE MECHANICS MODELS

Fatigue life of welded joints has been shown to consist mainly of crack growth
from pre-existing crack-like defects in the weld toe region [2,3]. In the
present study only the crack growth stage was considered, i.e. a possible crack
initiation stage was neglected.

An in-house computer program, CALPRED [7], was used for the fracture mechanics
calculations. Crack growth was assumed to follow the Paris-Erdogan type crack
growth law

$$\frac{da}{dN} = C(\Delta K)^m \qquad\qquad (1)$$

Crack growth of surface cracks was calculated in two directions - through thick-
ness at the deepest point and in the surface direction. A step-wise integration
of crack growth with updating of the aspect ratio $a/2c$ was applied. Numerical
tests showed that the procedure had satisfactory accuracy.

The parameters C and m of Eqn. (1) were assumed to be equal at all positions
along the crack front. Tests with simple specimens with semi-elliptical cracks,
however, have shown that the crack growth rate tends to be lower at the free
surface, most probably due to the larger plastic zone at this position [5].
This was taken into account by a reduction of the stress intensity factor K at
the free surface by a factor $F_c = 0.91$, accounting for the plane stress
condition at the surface.

The values of C and m were assumed as $C = 4.9 \cdot 10^{-12}$ [MPa $m^{1/2}$, m], $m = 3.1$.
These values fall within the scatterband of crack growth data for various struc-
tural steels [6] and are recommended for fracture mechanics analysis of crack
growth in welded steel structures [4].

In the analyses of the semi-elliptical cracks, i.e. stage I in Figs 3 and 4,
the stress intensity factor determined by Newman and Raju [8] was applied.

$$K = (\sigma_M + H\sigma_B) \sqrt{(\frac{\pi a}{Q})} \cdot F^{N-R} \tag{2}$$

The membrane and bendings stresses were obtained from shell analysis of the
specimens [9]. Eqn. (2) does not account for the local stress concentration and
corresponding nonlinear through thickness stress distribution at the weld toe.
This was included in the following manner. In the deepest point of the crack,
Eqn. (2) was used to account for the global stress concentration of the joint.
The additional notch stress distribution due to the local stress concentration
from the weld geometry was accounted for by the influence function method (point
load model) proposed by Albrecht and Yamada [10] and developed further by
Engesvik [11]. This leads to the resulting K in the deepest point.

$$K_{tot} = (\sigma_M + H\sigma_b)\sqrt{(\frac{\pi a}{Q})} \cdot F^{N-R} + \alpha_M \sigma_M \sqrt{(\pi a)} \cdot F^{A-Y} + \alpha_B \sigma_B \sqrt{(\pi a)} \cdot F^{A-Y} \tag{3}$$

$$\alpha_M = SCF_{M,weld} - 1$$

$F^{A-Y} = F_S \cdot F_T \cdot F_W \cdot F_E \cdot F_G$, corrections for geometry of crack, specimen,
stress distribution

In the surface width direction, the Newman-Raju solution was calculated using
the stresses at the crack tip location, including the global stress variation
from shell analysis, and the local stress concentration of the weld. The local
stress distribution in the weld toe region was determined by plane FEM analyses
with very small elements distributed through the thickness [9]. The parameters
describing the weld geometry, i.e. throat angle θ and toe radius ρ, were
obtained by measurements on the specimens.

For the analysis of through cracks, i.e. stage 2 in Figs 3 and 4, the solution
for K for through cracks with a straight crack front was employed [12]. The
loading was, however, separated in a nominal membrane stress which was constant
around the circumference and a varying membrane stress distribution around the
circumference due to reduction in stresses when the crack grew away from the
stress concentration of the stiffener.

$$K_{tot} = \sigma_M \sqrt{(\pi a)} + \alpha_{eq}\sigma_M \sqrt{(\pi a)} \cdot F_{G,through} \tag{4}$$

In the model the brace was assumed to be a plate of large width, hence the
finite width correction F_W was negligible. The K-solution given in Eqn. (4) is
limited to membrane stress. At the brace/column intersection, there were also
shell bending and weld notch stresses, cf. Fig. 5. The distribution of these
stresses was calculated around the circumference of the brace. An equivalent
membrane stress, which at each location around the circumference would give the
same cross sectional force as the total stress distribution, was calculated and
applied in Eqn. (4), see Fig. 5.

4. FRACTURE MECHANICS ANALYSIS AND DISCUSSION

4.1 Analysis of growth of semi-elliptical cracks

One of the major problems in fracture mechanics analysis of fatigue cracks initiating at weld toes, is the assessment of the size and shape of initial cracks. It has been demonstrated that crack-like defects in the weld toe region is an inherent feature of welds produced by conventional welding processes. These defects are non-metallic slag intrusions along the fusion line, formed when the metal is melted or pasty during welding. The size and shape of the defects have been found to be quite random, with typical depths in the range 0.05-0.4 mm [2,3].

In Fig. 6 are shown experimental crack shape data for brace/column weld cracks (Pos. 1) with fracture mechanics predictions assuming an initial crack $a_0/2c_0$ = 0.4/0.8. Similar data obtained for the gusset cracks (Pos. 2) are shown in Fig. 7.

In the analysis, growth of a single crack was modelled, i.e. the multiple crack initiation and crack coalesence effects were not taken into account. These effects were particularly pronounced at the brace/column weld (Fig. 6). For long cracks, the computational model and the test data appear to be converging towards an aspect ratio $a/2c$ in the range 0.2-0.3. In the initial stages of crack growth, however, there is a significant discrepancy.

The data from Pos. 2 (Fig. 7) were less affected by multiple initiation, and there is an overall agreement between analysis and experiments. However, the scatter in experimental data makes conclusions uncertain.

In Figs 8 og 9 are shown crack growth data and analysis for through thickness crack growth at the two positions of the model. With assumptions of an initial crack size within what has been reported for manual welds [2, 3], there is an overall agreement between tests and analysis. It is noted that at Pos. 1, the predictions tend to underestimate crack growth, i.e. good fit is obtained if a relatively large initial defect size to assumed. The reason for this is most probably the effects of crack coalescence, Fig. 6.

In similar analyses, using a forcing function for $a/2c$ in order to simulate crack coalescence, very good correlation between tests and analysis has been reported [11, 13]. However, in order to apply a forcing function, the experimental data for $a/2c$ need to be known a priory, making the method less of a predictive nature. Also shown in Fig. 8 is the effect of omitting the variation in stress around the circumference of the weld (dotted line), i.e. performing the analysis on the basis of the stress at Pos. 1.
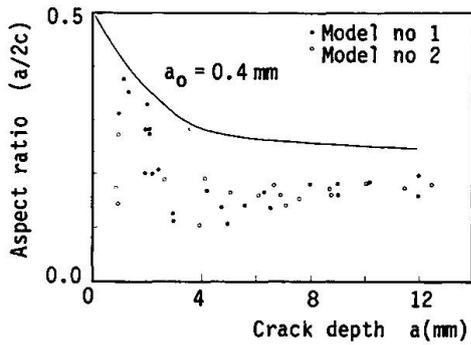
Figure 6   Crack shape data for part-through cracks at brace/column weld (Position ①, cf. Fig.1)
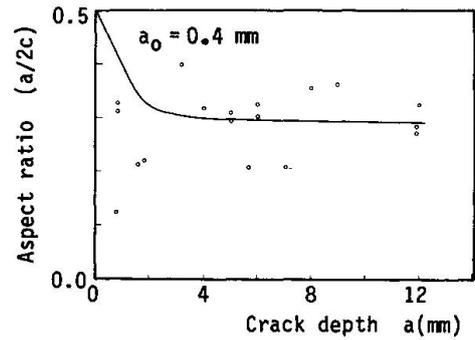
Figure 7   Crack shape data for part-through cracks at external stiffener welds (Position ②, cf. Fig.1)
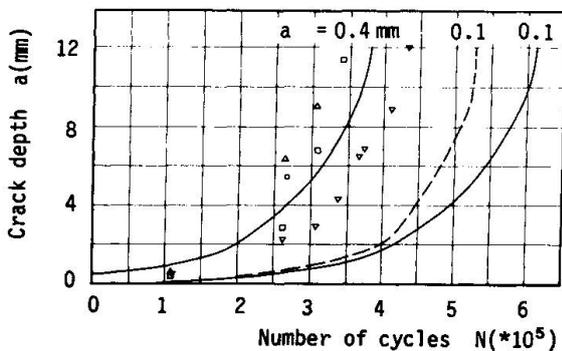
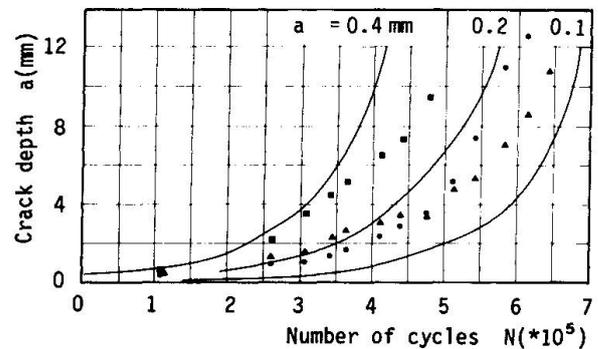Figure 8   Crack growth data for part-through cracks, position ①, model no. 2

Figure 9   Crack growth data for part-through cracks, position ②, cf. Fig.1

4.2   Analysis of through thickness cracks

In Fig. 10 the development of through cracks at the brace/column weld is shown. The transition from a semi-elliptical crack to a through crack was modelled by simply taking a straight crack front with a width equal to the surface width of the semi-elliptical crack at the stage of through thickness penetration. As seen from Fig. 3 the crack front is far from being straight due to the significant bending and notch stresses.

Two values for the initial through thickness crack size were employed. The top curve in Fig. 10 was obtained with the measured mean value of the width of the three cracks. The lower curve was obtained with the width of the computed crack, i.e. a computational model covering both stages of crack growth. This value was smaller than the measured ones due to an overestimated $a/2c$ - ratio in the calculation of semi-elliptical crack growth (Fig. 6). The figure shows that for cracks larger than ~ 150 mm, the computed crack growth rate is too high compared to the test results. This may be explained by the stress redistribution from the brace wall and into the stiffener. Since the computed results are based on the stresses in the original uncracked geometry, the redistribution is not accounted for.

In Fig. 11 the crack growth results of through thickness cracks at end of the
gusset (Pos. 2) are shown. In this case the initial crack width obtained from
the width of the semi-elliptical crack at through thickness corresponded closely
with the test results. The gusset weld and internal stiffener had only a local
influence on the crack growth at this position. For the through thickness crack
stage, the membrane stress in the chord wall was dominating, and the uncertainty
in modelling Eqn. 4 was much less than in the case of the brace/column weld.
Still, there is a significant difference between the computed and the measured
crack developments, underlining the assumption that load shedding effects are
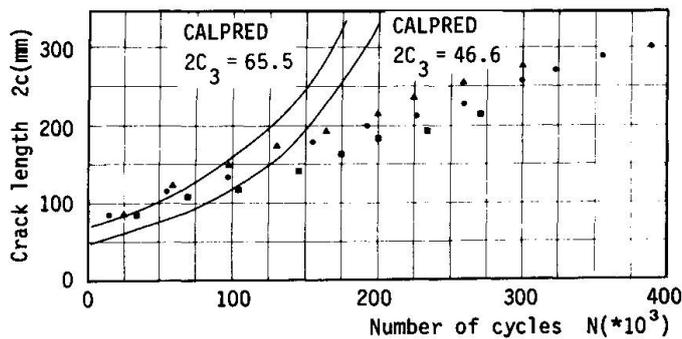important.

Figure 10   Crack growth data for through-thickness cracks,
             position ① , cf. Fig.1
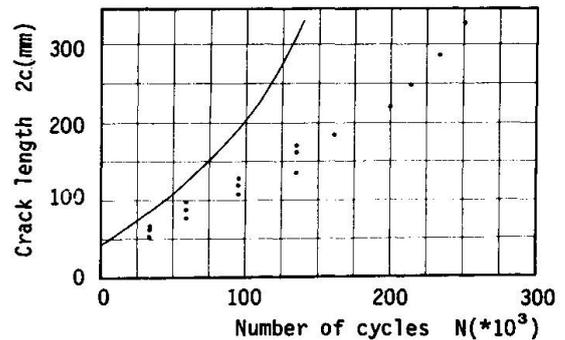
Figure 11   Crack growth data for through
             thickness cracks,
             position ② , cf. Fig.1

5. CONCLUSIONS

Fatigue crack growth in simplified but realistic models of brace/column connec-
tions typical of semi-submersible rigs was studied. A fracture mechanics model
was established in order to predict the observed crack growth behaviour. The
following observations were made,

- Significant multiple crack initiation occurred at hot spot regions of the
  brace/column welds. Crack coalescence occurred at a typical crack depth of
  3 mm, introducing a significant change in the crack shape development.
- For surface cracks, a two-parameter fracture mechanics model calculating crack
  shape development was established. Without taking crack coalescence into
  account, the model gave results in reasonable agreement with test data.
- At external gusset welds, multiple crack initiation was less pronounced.
  In this case, good agreement between predicted and experimental data was
  obtained for through thickness crack growth.

- After through thickness penetration, a significant residual fatigue life
  remained before catastrophic crack growth took place. For the brace/column
  weld, the total life was as much as 2.2 times the through thickness life. For
  the external gusset, the same factor was 1.6. Total life for both details was
  approximately the same.
- The predicted growth of through thickness cracks tended to underestimate
  residual life, probably due to load shedding effects which were not accounted
  for.

6.   REFERENCES

1.   EIDE, O.I. and BERGE, S.: Fatigue Capacity and Crack Growth in Stiffened
     Tubular Joints. SINTEF Report STF71 A89011, 1989. Also OMAE 1990.

2.   SIGNES, E.G. et al.: Factors Affecting Fatigue Strength of Welded High
     Strength Steels. British Welding Journal, March 1967.

3.   WATKINSON, F. et al.: The Fatigue Strength of Welded Joints in High
     Strength Steels and Methods for its Improvement. Proceeding Conference on
     Fatigue of Welded Structures, Brighton 1970.

4.   DnV Classification Note 30.2: Fatigue Strength Analysis for Mobile
     Offshore Units, 1984.

5.   RAJU, I.S. and NEWMAN, J.C.: An Empirical Stress Intensity Factor Equation
     for the Surface Crack. Eng. Fract. Mech., Vol. 15, pp. 185-192, 1981.

6.   ECSC Conference on Steel in Marine Structures, Institut de Recherches de la
     Siderurgie Francaise, Paris, 1981.

7.   SKALLERUD, B.: CALPRED, Computer Aided Life Predictions. SINTEF Report
     STF71 A89055, 1989.

8.   NEWMAN, J.C. and RAJU, I.S.: Stress Intensity Factor Equations for Cracks
     in Three-Dimensional Finite Bodies Subjected to Tension and Bending Loads.
     Chpt. 9 in Computational Methods in the Mechanics of Fracture, Ed. S.N.
     Atluri, Elsevier Science Publ. B.V., 1986.

9.   BRODTKORB, B.B.: Stress Analysis of a Tubular Joint with Internal
     Stiffening. SINTEF Report STF71 A89006, 1989.

10. ALBRECHT, P., YAMADA, K.: Rapid Calculation of Stress Intensity Factors.
     Jour. Struct. Div., ASCE, Vol. 103, pp. 377-389, 1977.

11   ENGESVIK, K.: Analysis of Uncertainties in the Fatigue Capacity of Welded
     Joints. Dr.ing. Thesis, The Norwegian Institute of Technology, Division of
     Marine Structures, 1982.

12. TADA, H., PARIS, P.C., IRWIN, G.R.: The Stress Analysis of Cracks,
     Handbook. Del Research Corp., 1985.

13. EIDE, O.I. and BERGE, S.: Fracture Mechanics Analysis of Welded Girders
     in Fatigue. Int. Conf. Fatigue of Welded Constructions, Brighton, 1987.

Remaining Fatigue Life of a Spherical Joint

Durée de vie restante d'un joint sphérique

Restlebensdauer sphärischer Knoten

Zdenek KNESL
Dr.
Inst. of Physical Metallurgy
Brno, Czechoslovakia

Zdenek Knesl, born 1940, received his degree in theoretical physics at the University of J.E. Purkyne in Brno. For ten years, he studied dislocation theory, and is currently applying numerical methods to fracture mechanics and fatigue-crack propagation.

Pavel MAREK
Assoc. Prof.
Sportovni stavby
Prague, Czechoslovakia

Pavel Marek, born 1932, received his civil engineering degree and PhD at the Czech Technical University in Prague. For 25 years, he did research and taught in structural steel at Czech and foreign Universities. At present, he is visiting professor at San Jose State University California.

Pavel POLCAR
Dr.
Inst. of Physical Metallurgy
Brno, Czechoslovakia

Pavel Polcar, born 1950, received his degree in mathematics at the University of J.E. Purkyne in Brno. For seven years he was involved in mathematical modelling of processes in rotary cement kilns. For the last eight years, he has taken part in various programming projects in continuum mechanics.

Milos VLK
Assoc. Prof.
Technical University
Brno, Czechoslovakia

Milos Vlk, born 1937, received his mechanical engineering degree and PhD at the Technical University in Brno. For 23 years, he has been engaged in problems of fatigue and brittle fracture and their applications to industrial practice. At present, he is a university teacher.

SUMMARY

The investigation of the remaining fatigue life of a spherical joint is based on the evaluation of a conical fatigue crack growing from the sphere to tube weld. An attempt is made to optimize the geometrical parameters of the joint in order to improve remaining fatigue life.

RÉSUMÉ

Le problème de la durée de vie restante d'un joint sphérique est basé sur l'évaluation d'une fissure de fatigue cônique se propageant depuis ce joint dans la soudure du tube. Une tentative d'optimisation des paramètres géométriques du joint a été faite dans le but d'en améliorer la durée de vie restante.

ZUSAMMENFASSUNG

Anhand der Beurteilung eines konischen Ermüdungsrisses, der von einer Kugel-Rohr-Schweissverbindung ausgeht, wird die Restlebensdauer eines sphärischen Knotens untersucht. Es wird versucht, die geometrische Form zu optimieren und dadurch die Ermüdungsfestigkeit solcher Verbindungen zu erhöhen.

1. INTRODUCTION

The Limit States Method, introduced in Czechoslovak Specifications for Structural Steel Design in 1969, was applied in case of dimensioning and reliability assessment of a 340 m high guyed latticed tubular steel TV mast located near Plzen. Special attention was paid to the investigation of the actual behaviour of welded joints (especially of the details like tubes welded to spherical nodes) exposed to fatigue. The information on response history, results of experimental investigation and on the final set up of the TV mast are discussed in [1].

The experimental study on fatigue strength of spherical joint was followed by a pilot study on crack propagation. The definition of the applied model based on the linear fracture mechanics and FEM is summarized in [2].

The steps following the pilot studies on the actual fatigue strength of spheric joints, mentioned above, were focused on the residual fatigue life and optimization of the geometrical proportion of spheric joint. The results are subject of this paper.

2. RESIDUAL FATIGUE LIFE OF THE CRACKED SPHERICAL JOINT

2.1 The formulation of the problem

In order fo formulate the problem, the experimental facts are summarized first:

During testing, the equivalent loading was represented by a force with amplitude of 350 kN and mean value of 250 kN. The crack was detected after 129 000 loading cycles and final fracture of the brittle type occured after approximately 150 000 loading cycles. On the basis of the fractographic study of the fractured surface of the failured spherical joint, the direction and the form of the fatigue crack were determined.

The sectional view of the spherical joint is given in Fig. 1. In accordance with the experimental set up, the boundary conditions for fatigue life calculations are modelled as follows (Fig.2): The external load is simulated by a constant stress σ acting on the tube in Z direction, the displacements in R direction equal to zero for the edge A and displacements in R direction equal to zero for the edge B of the sphere. The crack propagation direction is given by the angle α and crack grows along the surface of the cone created by rotation of the straight line p around the Z axes. The crack length a is measured along the straight line p (Fig.2).

On the basis of the above assumptions, the problem can be solved as an axialsymmetric one and for description of the stress state in the vicinity of the crack tip the plane strain approximation can be used.

In the following paragraphs the results are presented for the remaining fatigue life of the cracked spherical joint with the preexisting crack of the length a_0. The computation is based on

$$\frac{da}{dN} = C \cdot (\Delta K_I)^m \tag{1}$$

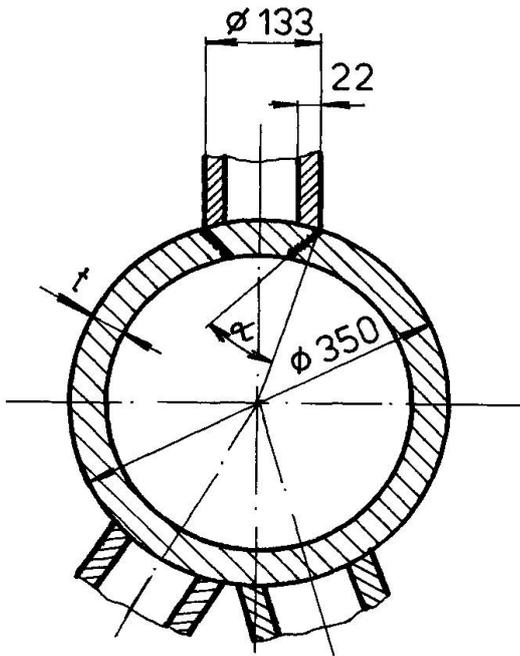where ΔK_I is a range of the stress intensity factor.

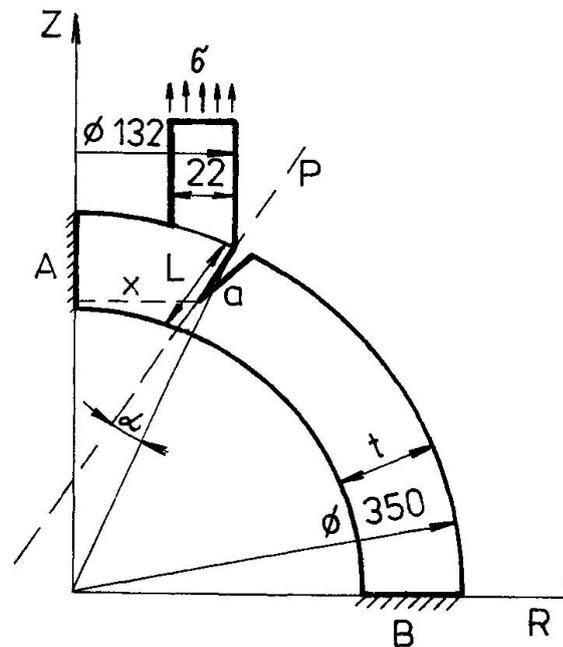**Fig.1** Sectional view of the spherical joint with conical crack

Fig.2 Numerical model used for FEM calculations

To this aim, the K_I calibration curve is calculated. Computations were performed by means of finite element method as implemented in PROKOP code [3].

2.2 K - calibration calculation

K - calibration curve, i.e. the dependence of the stress intensity factor K on the crack length a, was for our problem obtained by calculation of a strain energy release rate G(a)

$$G(a) = \delta U(a)/ \delta a ,\qquad (2)$$

where δa is a crack length increment causing a release of strain energy of amount δU. The stress intensity factors K_I (opening mode I) and K_{II} (shearing mode II) are directly related to the value of δU by equation (for plane strain)

$$G = (1 - \nu).(K_I^2 + K_{II}^2) / 2\mu ,\qquad (3)$$

where ν, μ are Poisson's ratio and shear modulus respectively.

K_I, K_{II} is calculated from (3) by means of procedure suggested in [3].

For δU calculation the method is used based on finite element design sensitivity analysis as implemented in PROKOP code [5].

The crack growth is modelled by means of a double noding technique [5]. The loading and boundary conditions correspond to those

formulated in 2.1.

The calculated K_I calibration curve can be approximated by the formula (for $0,15 \leqslant a/L \leqslant 0,8$)

$$K_I = 6. \sqrt{\pi a} . \left[8,178 \left(\frac{a}{L} \right)^{1/2} - 14,80 \left(\frac{a}{L} \right)^{3/2} + \right.$$

$$\left. + 11,13. \left(\frac{a}{L} \right)^{5/2} \right] , \tag{4}$$

where 6 is applied external stress acting on the tube (see Fig.2), $L = 34,61$ mm, $t = 30$ mm, $\alpha = 27^\circ$.

For the corresponding K_{II} value it holds (for $0,1 \leqslant a/L \leqslant 0,8$)

$$K_{II} \leqslant 0,06 \ K_I \tag{5}$$

and so K_{II} values have practically no influence on the fatigue crack propagation rate and on the remaining fatigue life as well.

2.3 Results

The remaining fatigue life N_f was then calculated by integration of Paris law (1) between initial crack size a_o and a chosen size a_f (for $m = 2,37$, $C = 5,70.10^{-11}$, da/dN [m/c], ΔK [MPa.m$^{1/2}$]) - see [2].

3. INFLUENCE OF THE SPHERICAL JOINT GEOMETRY

3.1 A fracture mechanics approach to the optimum design of structures [6]

In conventional strength calculations for loaded structures, usually the requirement is made, that a calculated stress should not exceed a critical value (e.g. design stress). If the main task of optimization is to improve conventional safety of the structure, the objective function is created from this point of view.

Evidently, in the case of structures weakened by cracks, the above conventional approach is no longer applicable and results of fracture mechanics should be taken into account.

The aim of the present chapter is to use the fracture mechanics as a tool for shape optimization of the spherical joint with respect to fatigue failure and remaining fatigue life.

3.2 Formulation of the optimization problem

The basic idea of fracture mechanics optimization is to decrease the probability of fracture by changes of geometry of structures under consideration.

The aim of our procedure is to increase the remaining fatigue life N_f (a_o, a_f) of the spherical joint.

The value of N_f depends on geometry of structure Γ, material properties M, history of the response of the structure to external loading F and boundary conditions B. For the given boundary conditions B, history of response F and material properties M the crack trajectory and, remaining fatigue life N_f as well, depends on the geometry of the structure only

$$N_f = N_f \cdot [A (\Gamma)] , \qquad (6)$$

where $A(\Gamma)$ describes the crack trajectory.

The optimization procedure can be formulated as

$$N_{max} = \max_{g_i} N_f [A (\Gamma)] , \qquad (7)$$

where set of parameters g_i (describing the geometry Γ) creates design variables

$$g_i \in \Gamma . \qquad (8)$$

Constraints for g_i follow from construction requirements and moreover have to prevent other types of construction collapse. In order to solve the problem, it is required with regard to each structure :

(1) To determine the initial crack propagation direction it may be supposed, that the location of the crack initiation is known.

(2) For the given initial crack to find numerically its trajectory $A(\Gamma)$ (i.e. crack propagation tracking).

(3) For the given crack trajectory $A(\Gamma)$ to calculate the values of the stress intensity factors (i.e. corresponding K - calibration curves) and remaining fatigue life N_f $[A(\Gamma)]$.

It is evident, that the formulated optimization problem is too complicated and cannot be completely solved. But, following the basic ideas of the procedure, some very useful conclusions for the design of structures can be obtained.

With respect to this fact, we have limited our considerations on the study of the influence of the sphere thickness t (see Fig.2) on the residual fatigue life N_f of the spherical joint. Supposing that the crack is initiated at the joining weld between tube and sphere, the dependence

$$N_f = N_f (t) \qquad (9)$$

can be calculated for particular orientation of crack - see next paragraph.

3.3 The orientation of the pre-existing crack

For the determination of the pre-existing crack orientation the energy criterion is used. Accordingly, the crack will propagate in direction $\alpha = \alpha_m$ identical to the direction of the minimum of the strain energy density w :

$$w (\alpha_m) = w_{min} (\alpha) . \qquad (10)$$

Strain energy density w is determined on the basis of finite element calculations and the eq. (10) is solved numerically. The computations were done for $a_o = 1,7$ mm.

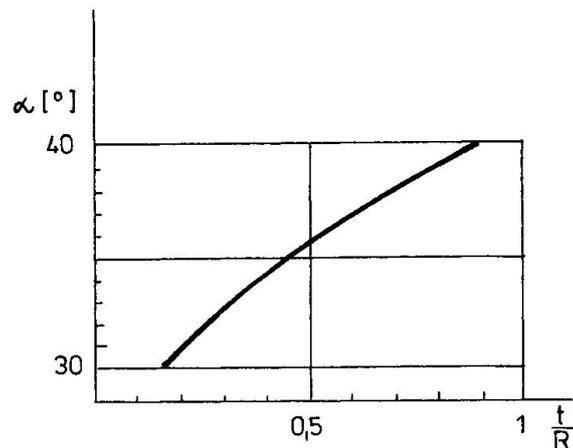As a result, the dependence $\alpha_m = \alpha_m(t)$ is given in Fig.3.

Fig.3 Dependence of crack propagation direction on sphere thickness   t   (R = radius of the sphere)

3.4 The determination of the fatigue crack trajectory

Generally, the fatigue crack initiated at the weld will propagate under mixed mode   I   and   II   conditions. In consequence of it, the crack trajectory have to be calculated first.

An essential ingredient of a crack propagation tracking is a criterion to predict the direction of crack propagation. Numerous past investigators have studied the problem, but there are still some disagreements among the various theoretical approaches (see e.g. [7]). In presented considerations, the strain energy density criterion as suggested by Sih - S criterion (e.g. [8]) is used. Following this criterion, the crack propagation direction depends on the ratio K_{II}/K_I and if $K_{II} \to 0$ the crack propagates directly along the straigt line.

For crack lengths in the interval $a_0 < a < 10$ mm, the ratio $K_{II}/K_I \leq 0,05$. So, as the first approximation let be supposed, that the crack trajectory is not influenced by mode II loading and crack propagates along the surface of the cone as in Chapter 2. Geometry of the cone is given by the value of $\alpha_m(t)$.

This approximation holds good for relatively short crack length (a ≤ 10 mm). For crack length a > 10 mm and especially for ratio t/R $\to 1$ (full sphere) and for more exact calculations the real crack path should be taken into account.

In the following paragraph it is supposed for all calculated cases, that the crack trajectory creates a cone. The changes of the sphere thickness   t   influence the angle α_m only.

3.5 K - calibration curves for spherical joint with different

sphere thickness

Based on the same procedure as in 2.2 the K_I calibration curves were calculated for various values of the sphere thickness t. Results hold in the crack length interval 1,7 mm to 25 mm.

3.6 Remaining fatigue life calculations

The remaining fatigue life N_f (a) is calculated by integration of Paris equation (1). As the ratio K_{II}/K_I changes slightly, K_I values can be taken as the parameter controlling the crack propagation rate. The value K_{II} has influence on the crack trajectory only [9].

3.7 Results

Using the same procedure and material characteristics as in the Chapter 2., the remaining fatigue life for various values of the sphere thickness (t = 30, 60, 90, 120, 150 mm) were calculated. To illustrate the influence of t on the remaining fatigue life of the spherical joint, the results for two limiting cases (t=30mm and t=150 mm) and initial crack length 2 mm and 15 mm are presented in the Fig. 4.
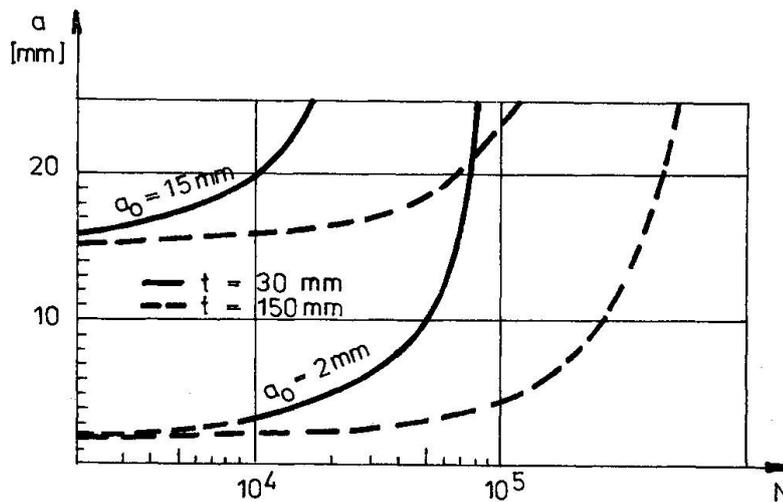

Fig.4 Remaining fatigue life of the spherical joint for two limiting thickesses t (a_o = initial crack length, N = number of cycles)

4. CONCLUSIONS

Linear elastic fracture mechanics and finite element method allow the evaluation of the remaining fatigue life of the spherical joint. With the aim to optimize the geometry of the joint, the influence of the sphere thickness on the fatigue life was studied. From this point of view, the full sphere of the joint gives the best results.

REFERENCES

1. MAREK P. - POVAŽAN J. - ŘEHOŘ P. - SCHRÁNIL J. - VLK M. - VOJTÍŠEK J., Investigation of Spherical Welded Joint of a Tubular Structure. In: Welding of Tubular Structures, Proceedings of 2nd Int.Conference IIW held in Boston, USA July 1984. Pergamon Press.

2. KNÉSL Z. - POLCAR P. - MAREK P. - VLK M., Analysis of Life of a Spherical Node by the Linear Fracture Mechanics Approach (in Czech). Zváranie 36, No 12, December 1987.

3. HOLUŠA L. et al., PROKOP-85. Research Report ÚFM ČSAV and OVC VUT (in Czech). Brno 1985.

4. KNÉSL Z., Determination of the Stress Intensity Factor for Mixed Mode by means of the Driving Force. Strojírenství 38, 1988, 163-166 (in Czech).

5. KNÉSL Z. - VRBKA J., The K Calculations by means of the Sensitivity Analysis. In: IV. Conference on Numerical Methods in Mechanics, Boboty 1989, p. 279-282 (in Czech).

6. KNÉSL Z. - VRBKA J., A fracture mechanics approach to the optimum design of structures. In: XI. Internationaler Kongress über Anwendungen der Mathematik in den Ingenieurwissenschaften, Weimar 1987, Berichte I, p.36-38.

7. WANG M.H., A modified S theory, Engng. Fract. Mech., 22,1985, 579.

8. SIH G.C., Strain-energy-density factor applied to mixed mode crack problems, Int. J. Fracture, 10, 1974, 305.

9. KNÉSL Z. - KUNZ L., A fatigue crack growth under mixed mode conditions. In: I. Conference on Mechanics, Praha 1987, (eds. J.Němec, R. Skrúcaný), vol. 4, p.127.